NTNU

Norwegian University of
Science and Technology

Cross-linked PEG/ ionic liquid composite membranes for CO2 separation

Junbo Yu

Chemical Engineering
Submission date: July 2018
Supervisor: Liyuan Deng, IKP
Co-supervisor: Jing Deng, IKP

Norwegian University of Science and Technology
Department of Chemical Engineering

Preface

I wish to express my sincere gratitude to my supervisor, Professor Liyuan Deng, for giving me a chance to join the Memfo group. I appreciate the opportunity as it helped me to learn more about membrane science.

Furthermore, I would like to thank my co-supervisor, Ph.D candidate Jing Deng, for her guidance and instruction. Her knowledge, expertise and encouragement helped me to understand concepts with a relative ease and gave me courage to overcome the difficulties.

Also, I am grateful to Dr. Zhongde Dai and Dr. Arne Lindbrathen. For helping me with the set up and for valuable suggestions.

A big thanks to all the group members from Memfo group. I really feel like we are in a family, “membrane family”. I received a lot of encouragement and advice during the group meetings which shaped this research.

Lastly, I’d like to thank to my parents and my friends. Your patience, support and company calmed me down when I was stressed and helped me to complete this report in time.

Abstract

The increasing CO_2 emission has become an urgent issue in the past decades. Comparing with other traditional CO_2 separation technologies such as amino absorption, membrane separation has been considered as a potential candidate, owing to its negligible pollution, low energy-consumption and low cost. Among the current membrane materials, PEO (polyethylene oxide)-based membranes have recently received a lot of attention due to their high affinity to CO_2. In Specialization Project TKP4580, a series of cross-linked PEG-based membrane containing dual cross-linking networks were developed. The object of this work is to further improve the CO_2/N_2 separation performance by physical blending with four different room temperature ionic liquids ([Bmim][BF_4], [Bmim][PF_6], [Bmim][Tf_2N] and [Bmim][TCM]).

The reaction mechanisms of aza-Michael addition and photo-polymerization which involved in membrane fabrication are confirmed by FT-IR test. The TGA results for the membranes exhibit a slight reduction in thermal stability by the addition of ionic liquids, but still qualify the industrial requirements of post-combustion for CO_2 capture. It can be concluded from DSC curves that the ionic liquids are well dispersed inside the membrane matrix and the polymer chains become more flexible. XRD results confirm that the composite membranes are in the amorphous state, and the crystallization is suppressed by IL addition.

The gas separation performance of these four composite membranes was tested by single gas permeation experiments. Results for all composite ionic liquid membranes have shown a decrease in CO_2 permeability at the low IL content of 20% and then it increases with addition of IL up to 80%. On the contrary, CO_2/N_2 ideal selectivity decreases with an increase in IL content from 0% to 80%. Upper bound was used to evaluate the gas separation performance of all IL-containing composite membranes. Among four ionic liquids, [Bmim][TCM] is the most effective in enhancing the CO_2/N_2 separation performance (CO_2 permeability of 138 Barrer, CO_2/N_2 selectivity of 45), compared with the neat membrane.

Table of contents

List of figures

List of tables

Nomenclature

Acronyms

CCS: Carbon Capture and Storage

ATRP: Atom transfer radical polymerization

DAE: Diaminoethane

DETA: Diethylenetriamine

DSC: Differential scanning calorimetry

EOR: Enhanced oil recovery

FT-IR: Fourier-transform infrared spectroscopy

GHG: Greenhouse Gas

HKPC: 1-Hydroxycyclohexyl phenylketone

IL: Ionic liquid

MEA: Mono ethanol amine

NOAA: National Oceanic and Atmospheric

PBT: Poly(butylene terephthalate)

PEG: Poly(ethylene glycol)

PEGDA: Poly(ethylene glycol diacrylate)

PEGMA: Poly(ethylene glycol) methacrylate

PEGDME: Poly(ethylene glycol) dimethyl ether

PEGMEA: Poly(ethylene glycol) methyl ether acrylate

PEO: Poly(ethylene oxide)

PES: Polyethersulfone

PILMs: Poly(ionic liquid) membranes

PS: Poly(styrene)

PSA: Pressure swing adsorption

PVC: Poly(viny chloride)

PVDF: Polyvinylidene fluoride

RTILs: Room temperature ionic liquids

SILMs: Supported ionic liquid membranes

SIPN: Semi-interpenetrating network

TAEA: Tris(2-aminoethyl)amine

T_d: Temperature of decomposition

TGA: Thermal gravimetric analysis

TSILs: Task-specific ionic liquids

UV: Ultraviolet

XLPEGDA: Crosslinked Poly(ethylene glycol diacrylate)

XRD: X-ray diffraction

Symbols

α: Selectivity

θ: Time lag

η_{IL}: Viscosity of the IL

Ω_{H2O}: Water uptake

A: Area of membrane

D: Diffusivity

D_T: Thermal diffusivity

D_{12}: CO_2 diffusivity in the IL

L: thickness of membrane

Mw: Molecular weight

p_d: Pressure of downstream

p_u: Pressure of upstream

P: Permeability

R: Ideal gas constant

S: Solubility

t: Time

T: Temperature

T_g: Glass transition temperature

W_d: Weight of dry sample

W_w: Weight of wet sample

V_{CO2}: Molar volume of CO_2

V_d: Volume of downstream

V_f: Free volume

1 Introduction

1.1 Global warming and CO_2 capture technology

Nowadays, global warming has become a serious concern in the modern society. Global warming is caused by the rapid growth of greenhouse gas level in the atmosphere. The greenhouse gas in the air absorbs the solar radiation, traps the heat reflected from the earth surface and keeps the earth warmer, leading to extreme weather, sea level rise and other long-term effects.

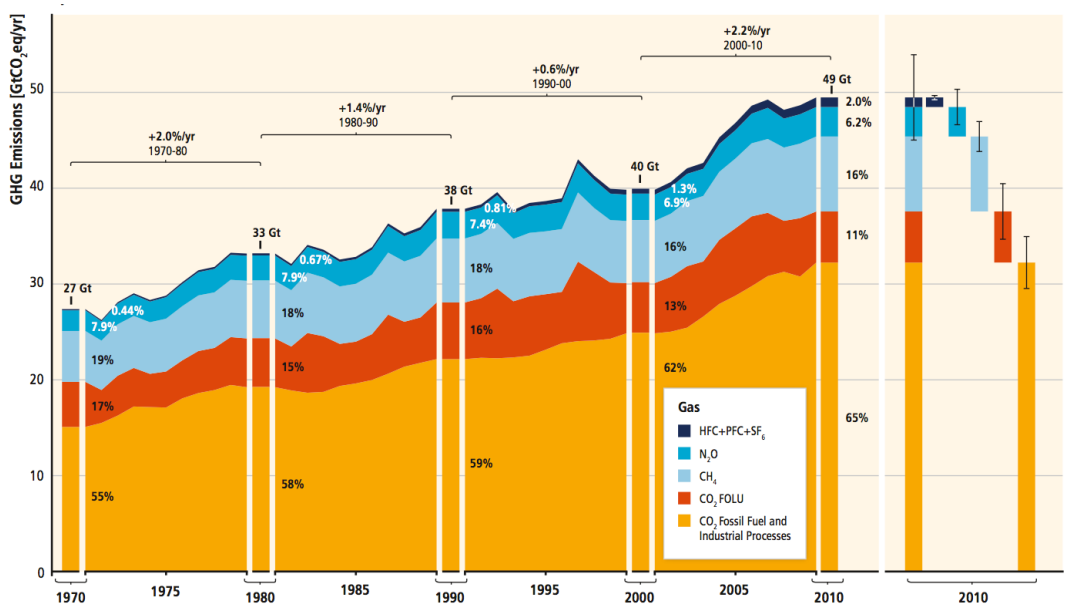

Figure 1.1 GHG(Greenhouse Gas) emissions data from 1970 to 2010(Change, 2014)

As shown in Figure 1.1, from 1970 to 2010, the GHG (Greenhouse Gas) emissions have been increased continually from 27 to 49 GtC yr^{-1} (Change, 2014), of which the main component is CO_2. Moreover, the percentage of CO_2 in the GHG Emissions has been increased from 55% to 65%. As a result, the atmospheric CO_2 level has been increased dramatically. Based on the data from NOAA (National Oceanic and Atmospheric Administration), until September 2017, the atmospheric CO_2 concentration has reached an extremely high level of 403.38 ppm, which reached the peak in human history (Dlugokencky, 2017).

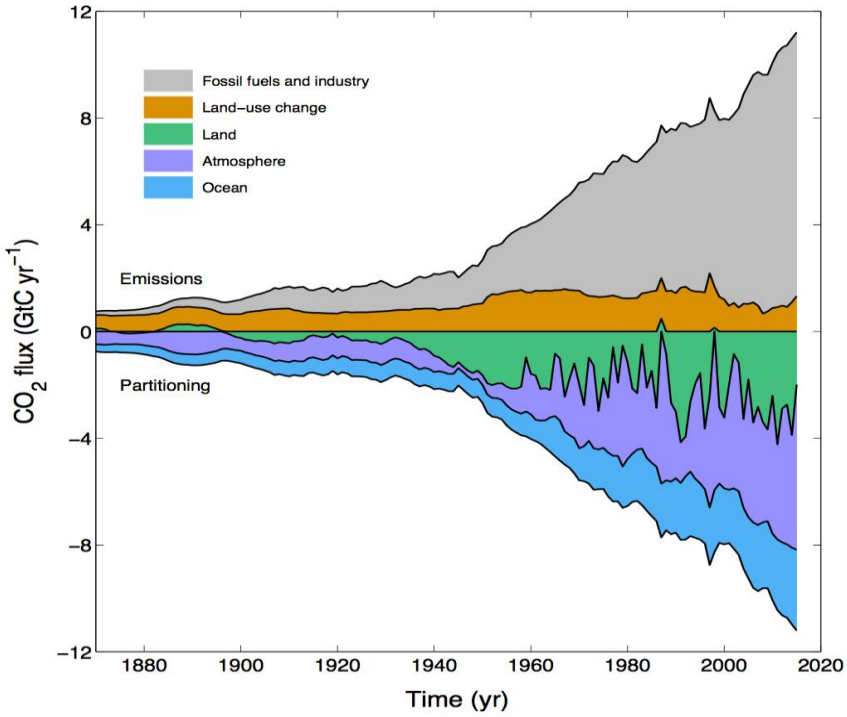

Figure 1.2 Components of the global carbon budget from 1870 to 2016 (Le Quéré et al., 2016)

From Figure 1.2, as can see, the GHG emissions from fossil fuel and industry increases rapidly, especially from 1960 to 2015. In last 10 years (2006-2015), 91% of the total GHG emissions came from fossil fuels combustion and the industry (Le Quéré et al., 2016). It is obvious that since the industrial revolution in the middle of 19 century, fossil fuels have become the dominant energy source and various industries have been developed explosively. With the development of science and technology, the quality of human life develops, but on the other hand, the demand for energy increases. To reduce GHG emissions, various low-carbon technologies (e.g., wind power, hydropower and nuclear power) have been developed. But before these new low carbon technologies become mature enough to replace the traditional technologies completely, fossil fuels will still be the main energy source in the foreseeable future (Wang et al., 2016). Hence,

the technologies reducing CO_2 emissions, such as Carbon Capture and Storage (CCS), have been attracted to the academic and the industrial. CCS technology includes separating CO_2 from large point sources, such as fossil fuel power stations and cement industry, compressing and transporting to storage sites where can isolate CO_2 from the atmosphere, and then storing it for hundreds of years. Employing CCS technology can prevent CO_2 emitting into the atmosphere from the fossil fuels power plant and industry successfully and efficiently.

There are several existing methods used to separate CO_2 from gas mixtures, such as conventional CO_2 absorption process, adsorption process, membrane separation and cryogenic distillation. Currently, the main source of CO_2 emission is the flue gas from the post-combustion process, which contains primarily N_2 and CO_2. The CO_2 concentration is about 10 to 15 vol. %. This means the promising CO_2 capture technology for flue gas has the capacity to handle a large amount of gas with low CO_2 partial pressure at an acceptable total cost containing the energy consumption and capital cost.

Conventional amine-based CO_2 absorption is the most mature CO_2 capture technology. It takes 90% of CO_2 separation market share (Zhongde Dai, Richard D. Noble, Douglas L. Gin, Xiangping Zhang, & Liyuan Deng, 2016a). The earliest commercial plants for capturing CO_2 in flue gas were built in the U.S. in the 1970s. But it was used in enhanced oil recovery (EOR) operation (Rao & Rubin, 2002). The first commercial CO_2 sequestration facility applied in CCS system was built in Norway for separating

and storing the CO_2 from Sleipner West gas filed in 1996(Rao & Rubin, 2002).

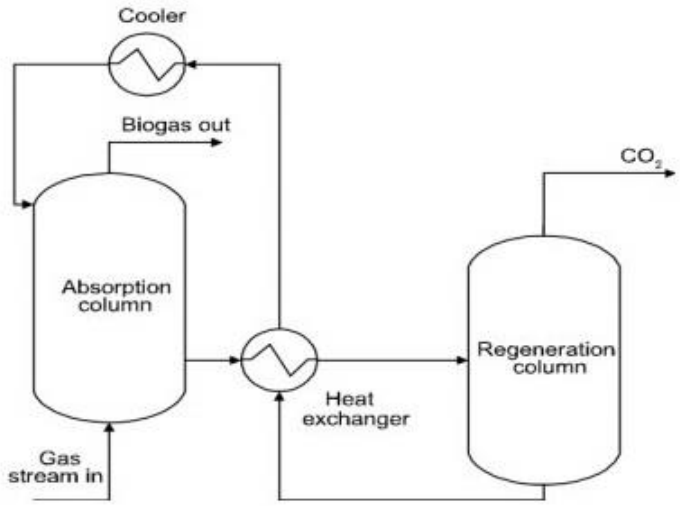

Figure 1.3 Flow chart for the MEA adsorption process
(Zhao, Leonhardt, MacConnell, Frear, & Chen, 2010)

Monoethanolamine (MEA) is the most widely used solvent to separate CO_2. As shown in Figure1.3, the typical process consists of 2 columns: absorption column and strip column. After absorbs CO_2 in the absorption column, MEA will be regenerated in the strip column and recycled to absorption column. Although this method is well established, it is highly energy demanding and needs high capital cost. The energy requirement and capital cost for CO_2 removal are 0.37 MWh/ton and 52$/ton respectively(Rochelle, 2009). Therefore, the solvent and process configurations need further development to reduce the capital investment and energy requirement.

Cryogenic distillation is a physical process that separate CO_2 from the mixed gas according to the difference between boiling points of gases. It operates under extremely low temperature and high pressure, which the high requirements need massive energy and high capital input. Thus, it is only used in some specific areas which need extremely

high purity and low temperature, like LNG production. However, it is not suited for post-combustion.

Pressure swing adsorption (PSA) is a physical adsorption method to separate CO_2 from flue gas at the elevated pressure. Adsorbents such as activated carbon, zeolite molecular sieves and carbon molecular sieves adsorb CO_2 under high pressure and desorb at low pressure. It is a novel approach for CO_2 capture but still facing challenges like high compression operation and the reliable material with affordable price.

Comparing to the methods mentioned above, membrane separation has gotten more and more attention from academia and industry because it is more environmental friendly, more energy-saving and lower capital and operating costs. More detailed introduction of membrane will be given in chapter 2. The properties of membrane material, such as gas separation properties, thermal stability, solubility and so on, are the key to the performance of membrane separation technology. Based on the material composition, membrane materials can be divided into three parts: polymeric membrane, inorganic membrane and polymer–inorganic hybrid membrane (Wang et al., 2016).

1.2 Poly(ethylene oxide)-based membranes

Among those current materials for gas separation membrane, poly(ethylene oxide) (PEO) membranes have shown their potential as a candidate. According to the research of Haiqing Lin et al(Lin & Freeman, 2004), PEO exhibits good performance on CO_2/N_2 separation. Due to the dipole-quadrupole interactions between polar ether group and

CO_2, PEO-based membranes have high CO_2/N_2 selectivity as well as high CO_2 permeability. Generally, PEO materials are in the rubbery state at the room temperature, suggesting the excellent gas transport properties. Although PEO-based polymers show good potential in CO_2/N_2 separation, they still have some drawbacks. The pure PEO polymers have high crystallinity and weak mechanical strength due to the hydrogen bonds between hydroxyl groups. To overcome these shortcomings, three different strategies (copolymerization, crosslinking and blending) have been investigated and shown their potential.

Copolymerization is a very common and useful strategy. Rigid segments have been copolymerized with PEG unit to improve material gas separation performance. Rigid segments and PEO segmental length are two important factors for material properties. The molecular length of PEO units has a strong effect on the physical property of the copolymers and gas separation performance (A. Car, C. Stropnik, W. Yave, & K. V. Peinemann, 2008). By introducing poly(butylene terephthalate), S.J.Metz et al (Metz, Mulder, & Wessling, 2004) synthesized poly(ethylene oxide) poly(butylene terephthalate) block copolymers and investigated its gas permeation properties. The CO_2 and N_2 permeabilities depended on the content of PBT and PEO segment length (Metz et al., 2004). Another copolymer called polyethylene oxide-b-polystyrene (PEO-b-PS) was synthesized by Xue et al (Xue et al., 2012). The coumarin groups from PS block arranged and formed into cylindrical phase structure(Xue et al., 2012), which leads to a high CO_2/N_2 separation performance. Dong and his coworkers (Dong et al.,

2016) report a high PEO content copolymer material P(PEGMA-co-DEAEMA-co-MMA). Because of the great amount of EO groups and amino groups, good performance was achieved (Dong et al., 2016). The membrane with 25 mol% of PEGMA has the best performance of excellent CO_2 permeability of 308 Barrer and acceptable CO_2/N_2 selectivity of 38 (Dong et al., 2016). The Poly(viny chloride) (PVC) as a widely used polymer are investigated for synthesizing the copolymer membranes due to its cheap price and good physical and chemical properties. Kim et al (Ahn, Seo, Kim, Ko, & Hong, 2009) synthesized amphiphilic graft copolymers poly(vinyl chloride)-graft-poly(oxyethylene methacrylate)(PVC-g-POEM) via atom transfer radical polymerization (ATRP). The PVC acts as the main chain, while the POEM behaves as the side chain. The PVC-g-POEM with 70 wt% of POEM has the highest CO_2 permeability of 100 Barrer which is 70 times higher than the pure PVC material (Ahn et al., 2009).

The second strategy is crosslinking. Several reaction mechanisms can be applied for membrane fabrications. For example, Lin et al (Lin, Kai, Freeman, Kalakkunnath, & Kalika, 2005) prepared cross-linked poly(ethylene glycol diacrylate) (PEGDA) by photo-polymerization. The PEG crosslinking networks were formed and crystallinity was suppressed. The CO_2 permeability of 138 Barrer and high CO_2/N_2 selectivity of 66 were achieved (Lin et al., 2005). Kwisnek et al (Kwisnek et al., 2014) developed a new family of crosslinked PEG-based membranes by using thiol−ene photo polymerization. Trithiol were used as a crosslinking agent and a thiol-ene network was formed. The

network crosslink density can be tuned by changing the amount of PEG dithiol in the formulation (Kwisnek et al., 2014). Moreover, thiol-functionalized polysiloxane was crosslinked with PEGDA by Kusuma et al (Kusuma et al., 2015). Compared to the cross-linked PEGDA, this new material's CO_2 permeability increases 75% with a slight reduction in CO_2/N_2 selectivity from 55 to 43 (Kusuma et al., 2015). Shao and his coworkers (Shao et al., 2013) synthesized a novel cross-linked PEO membranes by the reaction between the amino group of amino terminated Jeffamine and epoxy-terminated PEG monomer. A High CO_2 permeability of 144 Barrer and high CO_2/N_2 selectivity of 77 were achieved. With the same reaction mechanism, the same group (Quan et al., 2015) developed a bio-inspired CO2-philic network membrane by crosslinking bio-inspired dopamine with epoxy functional poly(ethylene oxide) (PEO). The CO_2 permeability and CO_2/N_2 selectivity of D-PEO membranes are 36.9 Barrer and 59.5 respectively (Quan et al., 2015). In general, the crystallization of PEO material could be suppressed by the crosslinking so the gas specimen could transport more effectively. However, the highly cross-linking density leads to a relatively low gas permeability and high selectivity caused by the reduction of chain mobility and decrease fractional free volume (FFV).

To improve the gas transport properties, physical blending with low molecular weight additives, such as PEG, ionic liquids(ILs) etc., has been introduced into the cross-linked PEO-based membranes. Many researchers blended PEG with commercial PEG-based copolymer Pebax® (Mannan et al., 2013). Feng et al (Feng et al., 2013) blended

poly(amide-12-b-ethylene oxide) (Pebax®1074) with poly(ethylene glycol) (PEG1500) and tested the gas separation performance at different temperatures. When the membranes are in the amorphous state, the permeability of CO_2 and selectivity of CO_2/N_2 both increase with the increment of the low-molecular-weight PEG content (Feng et al., 2013). The addition of PEG not only enhances the CO_2 solubility but also reduce the plasticization effect. Anja Car and her coworkers prepared Pebax®/polyethylene glycol (PEG) blend thin film composite membranes and tested at different conditions (A. Car, C. Stropnik, W. Yave, & K.-V. Peinemann, 2008). The results showed the CO_2 permeability of Pebax®/PEG blend membrane with 50 wt.% PEG content was two times higher than the neat Pebax® membrane due to the increment of CO_2 solubility by the incorporation of PEG. The selectivity of CO_2/N_2 is maintained at the same level without any significant decrease. The effect of different functional end-groups of the low-molecular-weight PEG on gas separation was also studied. Poly(ethylene glycol) dimethyl ether (PEGDME) was blended with Pebax® by Yave and his coworkers (Yave, Car, & Peinemann, 2010). The CO_2 permeability of composite membrane with the addition of 50 wt.% PEGDME significantly increased from 78 to 606 Barrer while the CO_2/N_2 selectivity slightly decrease from 49 to 43 (Yave et al., 2010).

Low molecular PEG can also be added into the crosslinked PEO-based membrane to further improve the crosslinked membrane performance. Quan and his co-workers incorporated PEGDME into the swollen dopamine/PEO network membranes and got

550% increment on CO_2 permeability with an acceptable decrease on selectivity from 59.5 to 45 (Quan et al., 2015). The great enhancement of performance is because of the higher EO content and inter-chain space caused by embedded PEGDME. Jiang et al developed semi-interpenetrating network (SIPN) membranes with excellent CO2/N_2 separation performance (Jiang, Li, & Shao, 2017). The cross-linked PEO backbone was built up by Poly(ethylene glycol) methyl ether acrylate (PEGMEA) with one acrylate groups and diacrylate functionalized PEGDA via one-step UV polymerization. In addition, the PEGDME was embedded into the cross-linked PEO network by physical blending (Jiang et al., 2017). The cross-linked composite membrane with 50 wt.% PEGDME has the highest CO_2 permeability of 2980 Barrer which is 520% higher than the neat cross-linked membrane without PEGDME (Jiang et al., 2017). The PEGDME embedment leads to the increasing chain flexibility and the facilitating gas diffusion, then resulting in the significant CO_2 permeability enhancement.

1.3 Ionic liquid and ionic liquid based membranes

Ionic liquid is defined as a salt with an organic cation and inorganic or organic anion, usually remaining liquid state at room temperature (Zhongde Dai, Richard D Noble, Douglas L Gin, Xiangping Zhang, & Liyuan Deng, 2016b). Owing to the unique physical and chemical properties, such as high CO_2 solubility, extremely low volatility and tunable chemical structure, ionic liquids have gotten more and more attention from the academia and industry. Blanchard et al (Blanchard, Gu, & Brennecke, 2001) firstly introduced ionic liquid into CO_2 capture as a separation medium. Compared to the

conventional organic solvents, ionic liquids have many advantages such as high thermal stability and negligible vapor pressure. But still some drawbacks need to be improved, for instance, high viscosity and expensive synthesis costs.

Based on the chemical structure, ionic liquids can be divided into two categories: room-temperature ionic liquids (RTILs) and task-specific ionic liquids (TSILs) (Dai et al., 2016b). Since four different RTILs will be utilized in this thesis, the review mainly focuses on the literature involved room-temperature ionic liquids in membrane area. RTILs is also called as the conventional ionic liquid because the solubility of the gas in the RTILs obeys Henry's law like typical physical solvents (Dai et al., 2016b). The Henry's constant is always employed to evaluate the gas absorption capacity of RTILs: the lower the Henry's constant is, the more gas the IL could absorb (Dai et al., 2016b). Based on the previous researches, it is found the solubility of CO_2 in RTIL depends on the anions much more than cations of ionic liquids. Table 1.1 presents Henry's constants for CO_2 in several conventional ionic liquids mostly used in literature.

Table 1.1 Henry's Constant for CO_2 in several ionic liquids (Zubeir et al., 2015)

Ionic liquid	*H* (bar)		
	10 °C	25 °C	50 °C
[Bmim][BF_4]	41.8	59	88.6
[Bmim][PF_6]	38.8	53.4	81.3
[Bmim][Tf_2N]	25.3	33	48.7
[Bmim][TCM]	36.2	48.4	75.4

These four ionic liquids share the same cation of $[Bmim]^+$, but with different anion. From the table 1.1, we can learn that at the room temperature, the CO_2 solubility

increase as follow: [Bmim][BF_4] < [Bmim][PF_6] < [Bmim][TCM] < [Bmim][Tf_2N] (Anthony, Anderson, Maginn, & Brennecke, 2005).

Table 1.2 Viscosities of these four conventional ionic liquids at 25 °C (Zubeir et al., 2015)

	[Bmim][BF_4]	[Bmim][PF_6]	[Bmim][Tf_2N]	[Bmim][TCM]
Viscosity/mPa·s	112	213	45	27.84

The viscosity of ionic liquids is another essential parameter when ionic liquids were utilized for gas absorption (Zubeir et al., 2015). The high viscosity of ionic liquid will cause high mass transfer resistance of gases dissolved in the ionic liquid and increase the energy consumption of pumping and mixing (Zubeir et al., 2015). The viscosity of four different ionic liquids is shown in Table 1.2. As observed from table 1.2, the CO_2 viscosity increase as follow: [Bmim][TCM] < [Bmim][Tf_2N] < [Bmim][BF_4] < [Bmim][PF_6]. Zubeir et al proposed a correlation between CO_2 diffusivity and viscosity for imidazolium-based ionic liquids. The correlation is shown below,

$$D_{12} = 2.66\times10^{-3}\frac{1}{\eta_{IL}^{0.66\pm0.03}V_{CO_2}^{1.04\pm0.08}} \tag{1.1}$$

where D_{12} is the CO_2 diffusivity in the IL, η_{IL} is the viscosity of the IL and V_{CO2} is the molar volume of CO_2 (Zubeir et al., 2015). Based on this correlation, it is clear that the viscosity has the negative effect on CO_2 absorption capacity. Combining Table 1.2, we can assume the [Bmim][TCM] may have the highest CO_2 diffusivity among these four ionic liquids considering the CO_2 absorption.

Due to the high CO_2 affinity and the neglect vapor pressure, a great number of efforts have been made by the researchers to integrate ionic liquid into membrane technology. During the last decade, different kinds of ionic liquid-based membranes have been developed. They are supported ionic liquid membranes (SILMs), poly(ionic liquid) membranes (PILMs) and polymer-ionic liquid composite membranes and so on.

By introducing the ionic liquid into the porous support, the SILMs can be prepared. The ionic liquid is immobilized in the pores of the porous support by capillary forces (Dai et al., 2016b). Comparing to the normal support liquid membranes (SLMs) with tradition solvent such as diaminoethane (DAE), diethylenetriamine (DETA), due to the negligible vapor pressure of ionic liquids, SILMs have much better stability. Ionic liquid zones could be formed in the support pores and the gas molecules dissolve into the ionic liquid zones, diffuse through the membrane and desorb to the other side. There are three ways to prepare SILMs, including direct immersion, vacuum and pressure. By employing different ionic liquids and porous supports, various SILMs with tunable performance have been fabricated. Scovazzo et al (Scovazzo et al., 2004) chose different ILs immersed in the hydrophilic polyethersulfone (PES). The results showed [Emim][dca]-membranes could reach a CO_2 permeability of 610 Barrer with a CO_2/N_2 selectivity of 61. Jindaratsamee and his coworkers applied hydrophobic polyvinylidene fluoride (PVDF) as porous support and synthesis supported microporous PVDF membrane with [Bmim][PF_6] and [Bmim][Tf_2N] (Jindaratsamee, Ito, Komuro, & Shimoyama, 2012). They found the fluorinated anions of ionic liquid play an important

role in the diffusion process as the carriers. The saturation of the carrier results in the reduction of CO_2 permeability at higher pressure difference and high CO_2 concentration. In order to further improve the SILMs performance, copper nanoparticles were incorporated as CO_2 carriers by Kang and his coworkers (Lee, Hong, Kim, Kang, & Kang, 2012). The CO_2 selectivity and CO_2 permeability both increased. Generally, the high CO2 permeability and moderate selectivity could be reached by SILM, even over the Upper bond, while the long-term stability under the relative high transmembrane pressure difference is the main constraint of SILMs.

To overcome the stability problem, researchers started blending the ionic liquid with the polymer to form polymer-ionic liquid composite membranes. Unlike SILMs, the fixed ionic liquids in the membranes matrix have a much higher stability facing high pressure. The interaction between the ionic liquid and polymer matrix stabilizing ionic liquid inside membrane could be both physical and chemical. Different combinations of ionic liquids and polymers have been proposed. With different polymers and ionic liquids, different results were obtained. The common commercial polymers have been employed in different works, such as poly(vinylidene difluoride) (PVDF), polyimide (PI) and polyether-polyamide block-copolymer (Pebax®). Due to the low cost, good mechanical strength and high chemical resistance, PVDF was investigated widely as host polymer. Chen et al (Chen, Li, & Chung, 2012) blended PVDF with low viscosity room temperature ionic liquid [Emim][$B(CN)_4$] and got high CO_2 permeability of 1778 Barrer and moderate CO_2/N_2 selectivity of 41.1. By incorporating [Emim][$B(CN)_4$],

four-folds enhancement in CO_2 permeability is obtained with simultaneously increasing CO_2 diffusivity and CO_2 solubility. Kanehashi and his coworkers (Kanehashi et al., 2013) blend glassy aromatic PI with [Bmim][Tf_2N] and prepared self-standing membranes by the solvent-casting method. Unlike the PVDF/IL composite membranes mentioned above, the CO_2 permeability firstly decreases within low ionic liquid content and then increases with further increasing ionic liquid loading. This may be because ionic liquid firstly occupies the free volume of PI and reduces the CO_2 diffusivity (Kanehashi et al., 2013). While with further increase of ionic liquid content, micro-sized domains of the IL are formed in the polymer matrix which provides less resistance for gas to transport through. Hence, CO_2 permeability shows this trend. Rabiee et al (Rabiee, Ghadimi, & Mohammadi, 2015) studied the CO_2/N_2 separation performance of poly(ether-b-amide6) (Pebax1657) /[Emim][BF_4] gel membranes. The results show with increasing the ionic liquid content, the CO_2 permeability increases from 94.80 to 492 Barrer with a slight decrease in selectivity from 74 to 61. The enhancement of CO_2 permeability may be ascribed to the plasticization effect led by the addition of ILs and then increase the chain flexibility as well as fraction free volume (FFV), which could benefit to a faster diffusion of gases.

1.4 Aim of the thesis

This thesis is based on the previous work from the TKP4580 specialization project done by the author. The cross-linked PEG-based membrane was prepared by introducing tris(2-aminoethyl)amine (TAEA) as the crosslinking agent. The effect of molecular

weight of PEGDA monomers and content of TAEA on membrane properties were investigated and analyzed. The results show the crystallinity of cross-linked PEG-based polymers is reduced and the gas separation performance is improved. Among all the cross-linked PEGDA membranes, XLPEGDA700/TAEA (6:1) has the best separation performance with the highest CO_2 permeability of 85.02 Barrer and highest selectivity of 63.5. The gas separation performance of XLPEGDA700/TAEA (6:1) could be further improved by blending with four different ionic liquids. Four kinds of cross-linked PEG/ionic liquid composite membranes will be fabricated and investigated. The reaction mechanisms will be verified by Fourier-transform infrared spectroscopy (FT-IR). The thermal stability, phase transition behavior, crystallization and hydrophilicity will be characterized by thermal gravimetric analysis (TGA), differential scanning calorimetry (DSC), X-ray diffraction (XRD) and water uptake experiment respectively. The performance of separation CO_2/N_2 will be tested in single gas permeation setups. The effect of different ionic liquids and effect of ionic liquid content will be investigated. The results will be discussed.

2 Theory

2.1 Membrane separation

Membrane is macroscopically defined as a selective barrier between two phases (Mulder, 2012). The membrane can separate different species from the mixture due to the difference between these species in molecular size, molecular shape or chemical structure. The driving force for the separation process can be pressure, concentration, temperature or electrical potential difference. According to different classification criteria, membrane can be classified into several different categories. For example, based on the material, membrane can be divided into organic membrane and inorganic membrane. While the most commonly used classification is based on the structure and separation mechanism.

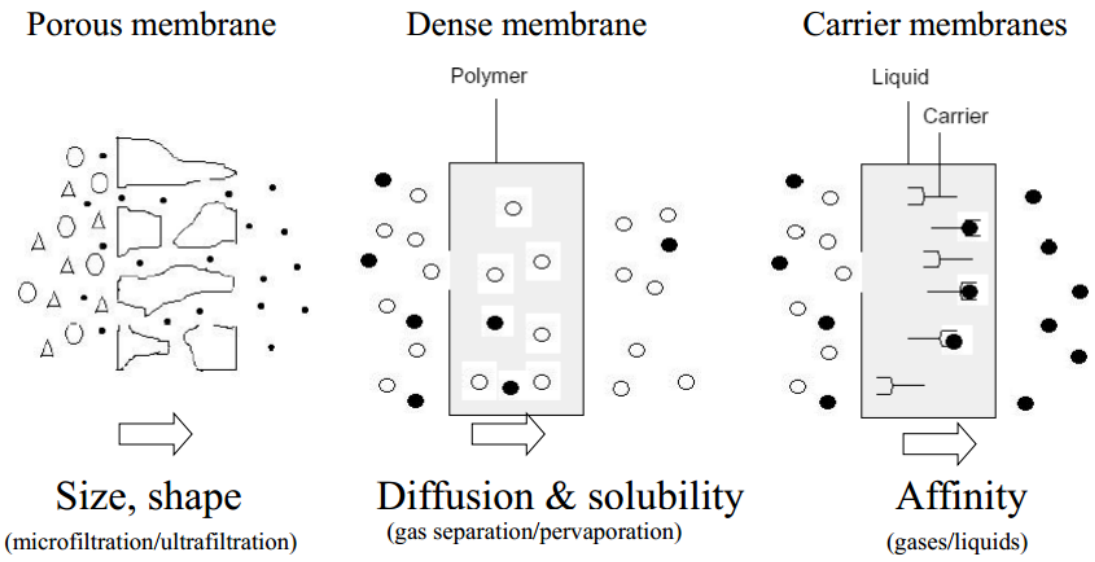

Figure 2.1 Schematic drawing of three basic types of membranes(Mulder, 2012)

The membranes can be categorized into three types, porous membrane, nonporous

membrane and carrier membrane. Figure 2.1 shows the schematic drawing of these three membranes with different transport mechanisms. For the porous membranes, there are three transport mechanisms based on the diameter of the pore, which are viscous flow (0.1 to 10μm), kundsen diffusion (20 Å to 0.1μm) and molecular sieving (5 to 20 Å) (Baker, 2004). About the nonporous membranes, solution-diffusion mechanism has been developed to describe the transport phenomenon. Facilitated transport mechanism explains the dynamic process of molecules goes through the membrane with the assist of the carrier. The driving force of the process is the carrier-gas concentration difference.

2.2 Polymeric membrane

Polymeric membranes usually are considered as nonporous, dense membranes in gas separation application. Since the molecular motion of an individual permeant molecule in the membrane matrix is totally random, it is difficult to describe the actual transport process. The solution-diffusion model simplified molecule transportation through the membrane into two steps. The first step is the dissolve of molecules into the upper layer of the membrane. The second step is the diffusion of the molecules through the membrane and release on the other side.

Permeability is the permeation rate of species to penetrate through the membra ne. Based on the solution-diffusion mechanism, the permeability P can be defi ned as the product of solubility S and diffusivity D (Mulder, 2012).

$$P = S \times D \tag{2.1}$$

Solubility is the number of molecules dissolved into the upper layer of the membrane at the equilibrium condition. It is a thermodynamic parameter. Diffusivity is the rate of which the penetrant can transport in the membrane. Unlike solubility, it is a kinetic parameter (Mulder, 2012).

Generally, selectivity was defined as

$$\alpha_{A/B} = \frac{y_A / y_B}{x_A / x_B} \tag{2.2}$$

Where y_A and y_B are the concentrations of components A and B in the feed stream and x_A and x_B are the concentrations of components A and B in the permeate stream.

For the ideal selectivity of the membrane for separating gas A and gas B can be calculated as below.

$$\alpha_{A/B} = \frac{P_A}{P_B} \tag{2.3}$$

Where P_A and P_B are the permeability of A and B respectively.

The selectivity and permeability are recognized as trade-off parameters. An increase in permeability of more permeable gas component usually leads to a decrease in selectivity. As a result, Robeson (Robeson, 2008) proposed an upper bound to describe this trade-off relationship. Figure 2.2 presents the upper bound correlation for the gas pair of CO_2/N_2 done reported in 2008. The black line shows the upper CO_2/N_2 separation performance of polymeric membranes and the red dots represent the published data

from different researchers up to 2008.

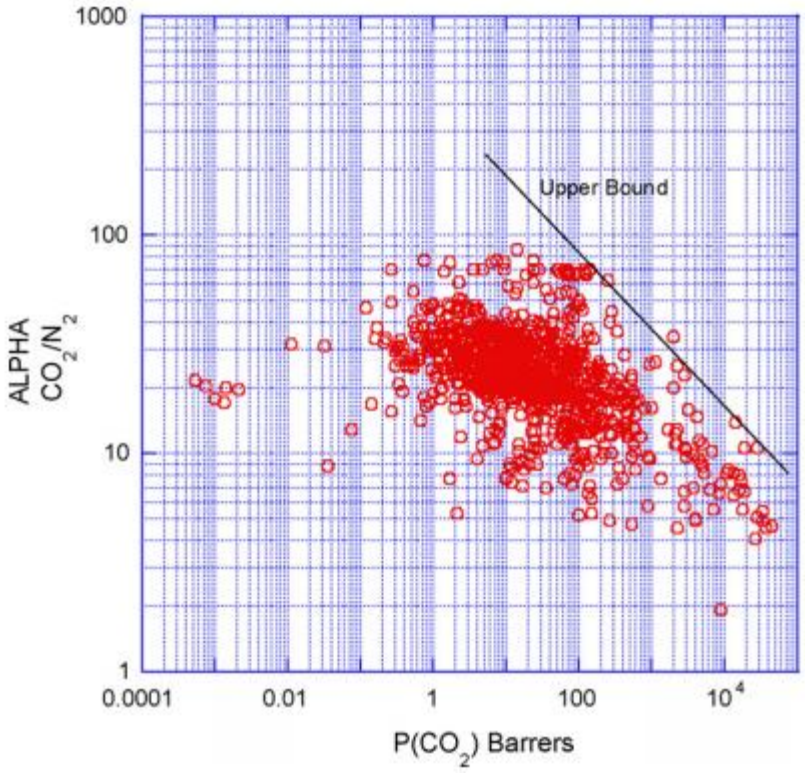

Figure 2.2 Upper bound correlation for CO_2/N_2 separation (Robeson, 2008)

The upper right corner is considered as attractive zone because of the high CO_2 permeability and high CO_2/N_2 selectivity.

2.3 Polymer material property

For the nonporous polymeric membranes, the permeation, mechanical and chemical properties are strongly affected by the state of the polymer. There are two very important parameters. For the amorphous polymer, there are two states. One is the glassy state, the other is the rubbery state. The temperature of the phase transition is called glass transition temperature T_g. Figure 2.3 shows the variation of tensile modulus E with temperature. The tensile modulus of the glassy state is often 3 to 4 orders

magnitude higher than that of rubbery state.

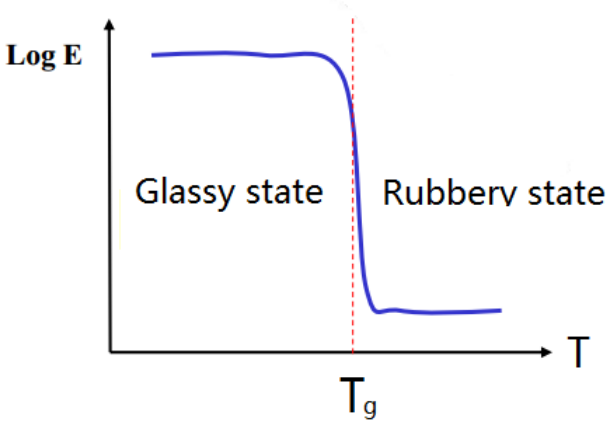

Figure 2.3 Tensile modulus E as a function of temperature(Mulder, 2012)

Free volume is defined as the volume unoccupied by the polymer chains. The free volume varied with temperature is shown in Figure 2.3.

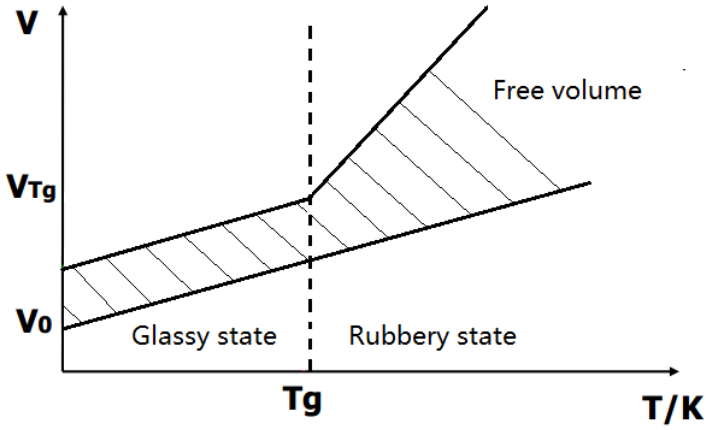

Figure 2.4 Free volume as a function of temperature for different phase states(Mulder, 2012)

The free volume in the glassy state is constant because the polymer chains are fixed in a certain region and segmental mobility is suppressed (White & Lipson, 2016). As a result, the polymer material in glassy state is tough and brittle. When the polymer is in the rubbery state, the polymer chains are flexible, the chain mobility increases.

Therefore, the polymer material at rubbery state is relatively soft and flexible. The free volume at rubbery state is a function of temperature and shown as below (Mulder, 2012).

$$V_f = V_{f,T_g} + \Delta\alpha(T - T_g) \tag{2.4}$$

Where V_f is the free volume, $V_{f,Tg}$ is the free volume, T is the temperature and T_g is the glass transition temperature. With increasing the temperature, free volume increases. The free volume theory associated free volume with diffusion coefficient. The thermodynamic diffusion coefficient can be calculated by Equation 2.5 according to the theory (Mulder, 2012).

$$D_T = RTA_f \exp(-\frac{B}{V_f}) \tag{2.5}$$

Where D_T is the thermal diffusivity coefficient, B is the minimal local free volume for penetrant to pass through, R is the ideal gas constant, T is the temperature and V_f is the free volume. This equation showed that the diffusion coefficient increases with the increase of free volume and decrease of penetrant molecular size.

3 Experiment

This chapter describes the membrane preparation and several characterization methods for reaction mechanisms, thermal properties, phase transition, crystallinity, hydrophilicity and gas separation performance.

3.1 Material

3.1.1 General chemicals

Poly(ethylene glycol) diacrylate with different molecular weight (PEGDA, Mw=250 , 575 and 700 g/mol) were purchased from Sigma-Aldrich. Tris(2-aminoethyl)amine (TAEA, Mw=146.23 g/mol) as cross-linking agent was bought from Sigma-Aldrich. The chemical structure of PEGDA and TAEA are presented in Figure 3.1. The 1-hydroxycyclohexyl phenyl ketone (HCPK, Mw=204.26 g/mol) working as the photo-initiator was purchased from Sigma-Aldrich. The pure gases (N_2 and CO_2) used in the single gas permeation test were provided by AGA.

PEGDA:

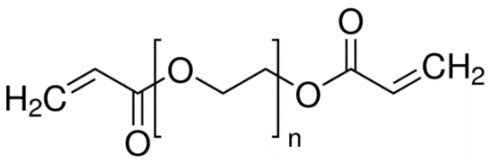

TAEA:

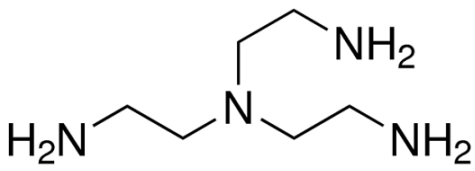

Figure 3.1 Chemical structure of PEGDA and TAEA

3.1.2 Ionic liquids

1-Butyl-3-methylimidazolium bis(trifluoromethylsulfonyl)imide ([Bmim][Tf_2N] , ⩾ 98%), 1-Butyl-3-methylimidazolium tetrafluorobotate ([Bmim][BF_4] , ⩾98%) and 1-Butyl-3-methylimidazolium hexafluorophosphate ([Bmim][PF_6], ⩾ 98%) were purchased from Sigma-Aldrich. 1-Butyl-3-methylimidazolium tricyanomethanide ([Bmim][TCM], ⩾ 98%) were bought from Iolitec (Germany). The chemical structures of 4 ionic liquids are depicted in figure 3.2.

A: Cation group

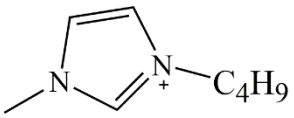

$[Bmim]^+$

B: Anion group

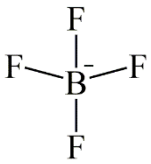

$[BF_4]^-$

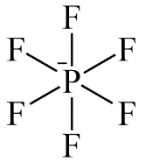

$[PF_6]^-$

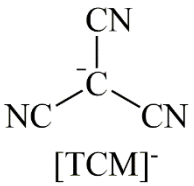

$[TCM]^-$

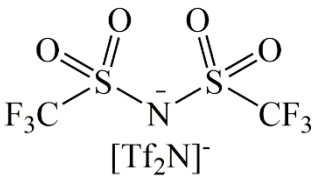

$[Tf_2N]^-$

Figure 3.2 Chemical structures of [Bmim][BF_4], [Bmim][PF_6], [Bmim][Tf_2N] and [Bmim][TCM]

3.2 Membrane preparation

The membranes were prepared in three steps. First, PEGDA, a desired amount of ionic

liquid and HCPK (0.01-0.1 wt% of PEGDA) were mixed on the magnetic stirrer for 30 minutes. The membrane solution after well mixing was homogeneous. Second, the desired amount TAEA was added into the PEGDA-ionic liquid solution and magnetically stirred for another 30 minutes at room temperature. The aza-Michael addition reaction between PEGDA and TAEA occurred in this step.

To remove the possible bubbles from the solution, the solution after mixing was put into a vacuum oven and vacuumed for 10 minutes. Afterward, the solution was carefully poured on a clean quartz plate. Another clean quartz plate was placed on the top of the solution. The solution was in the gap of two quartz plates like a sandwich. Two spacers were also put between the plates to control the membrane thickness between 250 to 300 μm. Then the two plates with solution were put into a homemade UV box and exposed under UV light of 365 nm wavelength and 4 $mWcm^{-2}$ of intensity for 2 hours for the photo- polymerization.

In this work, the content of ILs is defined as the mass ratio between ionic liquid and PEGDA. The notation used in this paper reflects the name of the ionic liquid, membrane matrix and ionic liquid content. For instance, formulations PEGDA/[Bmim][TCM] (40%) means cross-linked PEGDA as the polymer matrix is blended with [Bmim][TCM] and the mass of ionic liquid is 40% of PEGDA.

3.3 Membrane characterization

3.3.1 Fourier transform infrared spectroscopy (FT-IR)

Fourier transform infrared spectroscopy (FT-IR) was used to identify the composition of the samples. For organic molecules, the atoms formed chemical bonds is vibrating at the certain frequencies. Hence, when the organic materials are irradiated by the infrared light, the chemical bonds will have absorption infrared light at certain wavenumbers. Different chemical bonds or functional groups have different absorption frequencies. It locates in different positions in the infrared spectrum. Based on the spectrum, the composition of the sample can be analyzed, as well as the reaction mechanism. Thermo Scientific Nicolet™ iS™ 50 FT-IR Spectrometer was used for the FTIR analysis to confirm the reaction mechanism involved.

3.3.2 Differential scanning calorimetry (DSC)

Differential scanning calorimetry (DSC) is a technique usually used to investigate the phase transition of polymers. When the sample undergoes a phase transition, it will absorb or release certain amount of heat, which can be monitored by the DSC. Glass transition temperature can be obtained by analyzing the DSC curve. The analysis was performed by using a DSC 214 Polyma from NETZSCH-Gerätebau GmbH. The temperature range for all membranes was set from -100°C to 150°C with a constant heating rate of 10°C /min under N_2 atmosphere.

3.3.3 Thermal gravimetric analysis (TGA)

Thermal gravimetric analysis (TGA) is a method of analyzing the thermal stability of samples. The temperature in the furnace can be controlled by the program. The weight of the sample was recorded with changing the temperature of the furnace. The thermal decomposition temperature can be recognized in the result by a significant mass loss. A thermal gravimetric analyzer TG 209 F1 Libra from NETZSCH-Gerätebau GmbH was used for analyzing all the membranes. For all the test, the testing temperature range was programed from 25°C to 700°C with a constant heating rate of 10°C /min under N_2 atmosphere.

3.3.4 X-ray diffraction (XRD)

X-ray diffraction (XRD) is a method for studying the crystallinity of the polymeric membranes. By analyzing the diffraction versus intensity curve, the degree of crystallinity can be obtained. All the samples were tested by Focus D8 x-Ray Diffractometer. The diffraction angle was set from 5° to 75°.

3.3.5 Water-uptake

Water-uptake test is a method for investigating the hydrophilicity of the membranes. The test was performed as follow. All the membrane samples were put into the vacuum oven dried for 24 hours before water uptake test to make sure there was no water vapor dissolved in the membranes. Then, dry membranes were put into a hermetically closed

water desiccator. Water was filled in the bottom of the water desiccator to ensure the water vapor was saturated. The weight of the samples was measured every 24 hours until it stayed stable. The water uptake Ω_{H2O} of membranes was calculated by Equation 3.1.

$$\Omega_{H_2O} = \frac{W_w - W_d}{W_d} \times 100\% \quad (3.1)$$

Where W_w is the weight of wet sample and W_d is the weight of dry sample.

3.3.6 Single gas permeation test

The gas separation performance of the membranes was tested by the single gas permeation set-up. The flow sheet of the set-up was presented in Figure 3.3.

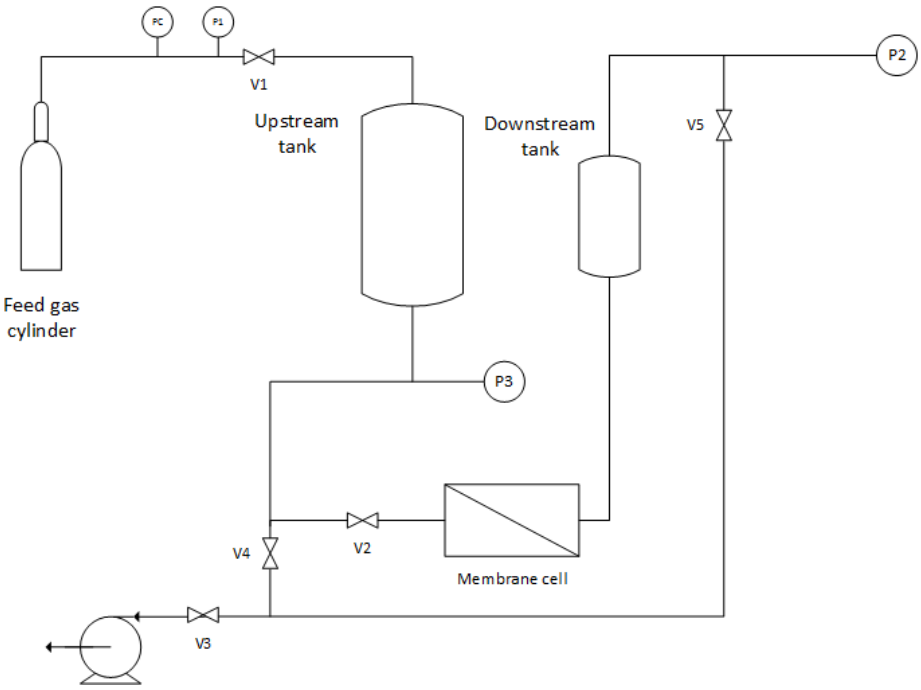

Figure 3.3 Schematic drawing of single gas permeation set-up

The set-up is mainly consisting of an upstream tank for feed gas, a membrane module

and a downstream tank. The pressure of both up and downstream tank was measured by two pressure indicators. Before starting the test, the membrane was put into membrane module and fully vacuumed, as well as the downstream and upstream tank, for at least 6 hours. The effect of penetrant dissolved in the membrane or present in downstream or upstream was eliminated. After that, the upstream tank was filled with specific gas (CO_2 and N_2 in this project). The upstream pressure was controlled around 2 bars. The single gas permeation test started at the moment when the upstream tank and membrane module was connected. The pressures of the upstream and downstream tank were recorded by the computer. Before all the test, to eliminate the system error, leakage test for the whole set-up was made. By combining definition of permeability and ideal gas law, the permeability is given by Equation 3.2.

$$P = \left[\left(\frac{dp_d}{dt} \right)_{steady\ state} - \left(\frac{dp_d}{dt} \right)_{leakage} \right] \times \frac{V_d}{A \times R \times T} \times \frac{l}{(p_u - p_d)} \tag{3.2}$$

Where P is the gas permeability, R is the ideal gas constant, V_d is the downstream volume, A is the membrane area, T is the operating temperature, l is the membrane thickness and p_d and p_u are the pressures of the downstream tank and upstream tank respectively.

$(dp_d / dt)_{steady\ state}$ is the slope of downstream pressure at the steady state.

$(dp_d / dt)_{leakage}$ is the leakage rate obtained from the leakage test for the whole system.

The ideal selectivity was calculated by

$$\alpha = \frac{P_{CO2}}{P_{N2}} \tag{3.3}$$

Where P_{CO2} and P_{N2} are the permeability of CO_2 and N_2 respectively.

Time lag method was applied to calculate the diffusivity of CO_2. As shown in Figure 3.4, the time lag can be obtained from the intercept of the linear plot of $Q_t/(l,c)$ versus t.

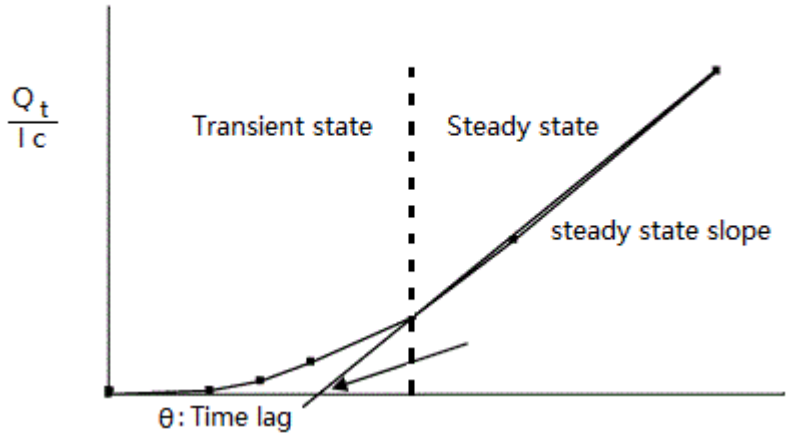

Figure 3.4 illustration of time-lag method

By applying equation shown below, diffusivity D can be calculated.

$$D = \frac{l^2}{6\theta} \tag{3.4}$$

According to Equation 2.1, solubility can be determined by the ratio of permeability and diffusivity.

$$S = \frac{P}{D} \tag{3.5}$$

4 Result and discussion

4.1 FT-IR results

Fourier transform infrared spectroscopy (FT-IR) was used to verify and confirm the reaction mechanisms of two crosslinking relations and analysis the PEGDA/IL composite membranes structure. The FT-IR results will be presented in two parts: confirming the mechanisms of cross-linking reactions used in current work and analyzing the structure of composite membranes.

4.1.1 Crosslinking reaction mechanism confirmation

Two reactions are involved in the preparation of the composite membranes. The first one is the aza-Michel addition, which refers to the reaction between the N-H bond and acrylate groups. In this research, acrylate groups from PEGDA are excessive. Hence, after the first stage, all the N-H bonds and equivalent C=C bonds are consumed. Then, the unreacted acrylate groups will be homo-polymerized under UV irradiation during the second stage.

To confirm the reaction mechanisms of these two cross-linking reactions for all composite membranes, the FT-IR spectrums of PEGDA, TAEA, selected ionic liquids and final membranes are conducted. The confirmation of crosslinking reaction mechanisms is performed by analyzing the results of PEGDA composite membrane with 40% [Bmim][BF_4] weight ratio as an example.

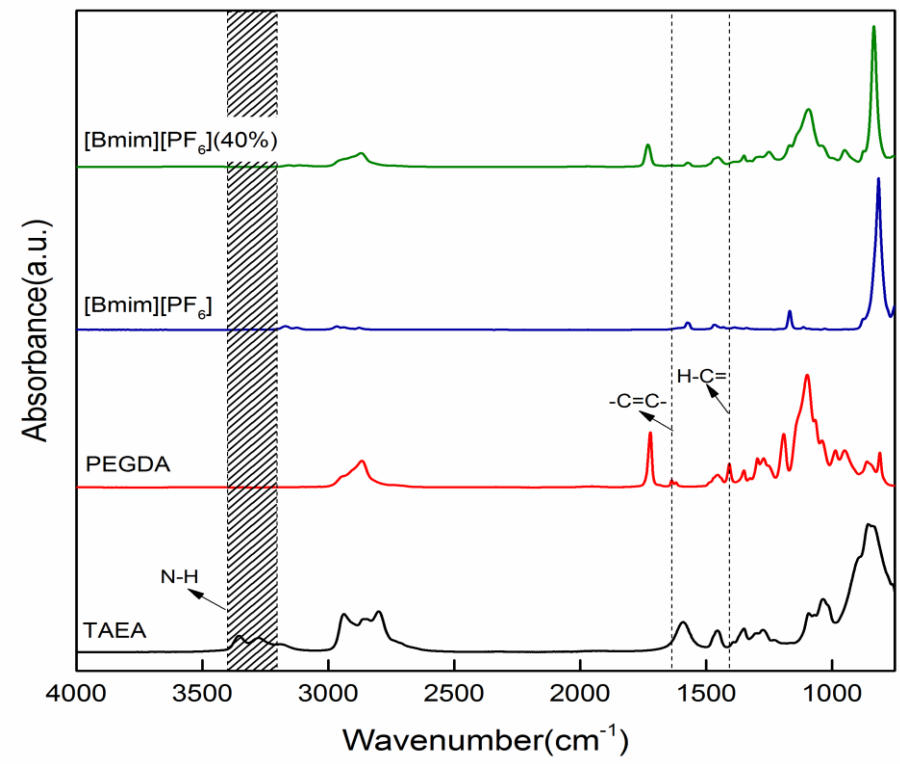

Figure 4.1 FT-IR result of PEGDA/[Bmim][BF_4](40%) membrane for confirmation the reaction mechanisms

Figure 4.1 shows the FT-IR spectrum of PEGDA, TAEA, pure [Bmim][BF_4] and hybrid PEGDA/[Bmim][BF_4](40%) membrane. The peak exists from 3200 cm^{-1} to 3400 cm^{-1} of TAEA is associated with N-H vibrations from amine groups. The acrylate groups of PEGDA have two characteristic peaks at 1631 cm^{-1} and 1410 cm^{-1}, respectively. The peak at 1631 cm^{-1} is corresponding to the -C=C-, while the peak at 1410 cm^{-1} is related to the H-C=.

As described in Chapter 3, [Bmim][BF_4] is firstly blended with PEGDA and initiator, followed by TAEA. Aza-Michael addition happens between primary amine groups of TAEA and acrylate groups of PEGDA. Compared with the spectrum of composite membrane and TAEA, the peak of N-H bonds (3200-3400 cm^{-1}) coming from TAEA

disappeared. This phenomenon indicates that the aza-Michael addition was achieved. After blending TAEA with PEGDA and [Bmim][BF_4], the well-mixed solution was poured between two clean quartz plates and exposed under UV light for 2 hours. In addition, the peaks of -C=C- (1637 cm^{-1} and 1410 cm^{-1}) from PEGDA completely disappeared in the spectra of the final membrane, demonstrating all acrylate groups were well reacted during aza-Michael addition stage and UV curing stage. Finally, the achievement of the dual-crosslink networks took place.

4.1.2 FT-IR result of membranes with [Bmim][BF_4]

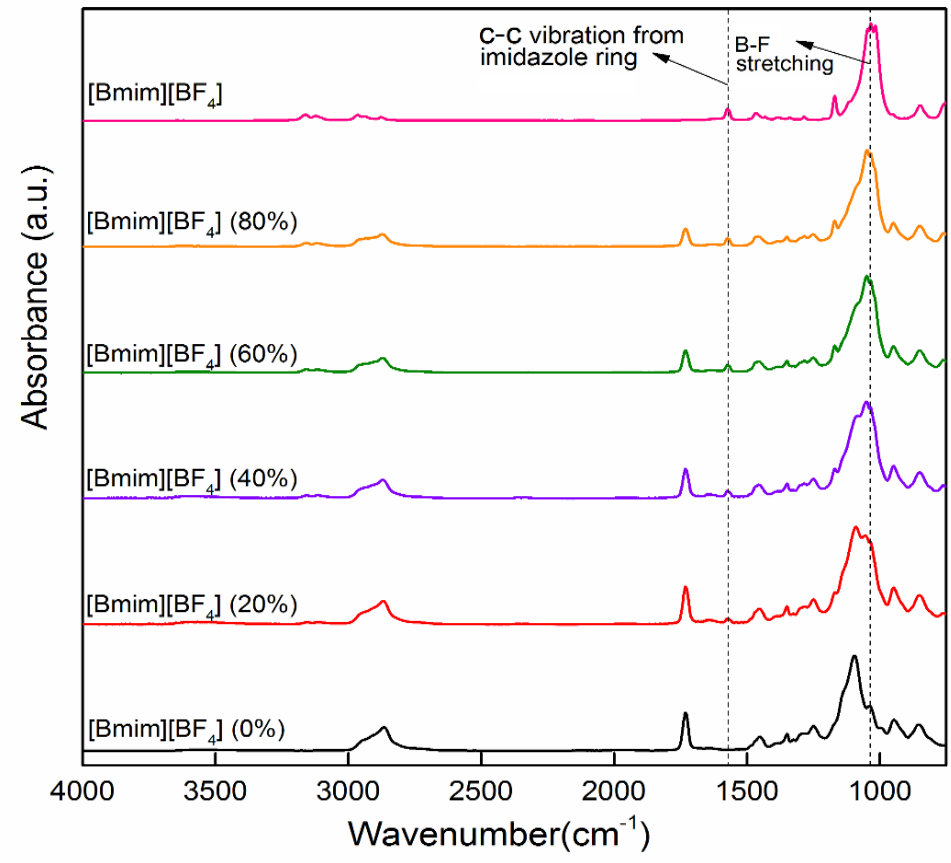

Figure 4.2 FT-IR result of PEGDA/[Bmim][BF_4] membrane with different [Bmim][BF_4] content

The FT-IR spectrums of the cross-linked PEGDA/TAEA membranes with different content of [Bmim][BF_4] are presented in Fig. 4.2. For pure [Bmim][BF_4], the bands between 1550 and 1600 cm^{-1} are assigned to C-C vibration of the imidazole ring, whereas the strong multimodal peak between 1150 to 1050 cm^{-1} is attributed to B-F stretching in $[BF_4]^-$. Firstly, compared the neat cross-linked PEGDA membrane with PEGDA/[Bmim][BF_4] composite membrane, we found that no new peaks have appeared. Considering the chemical structure of ILs and monomers, it can be inferred that there is no chemical reaction between the polymer matrix and IL. Then next, as presented in the figure above, the intensities of both peaks increase with the increment of [Bmim][BF_4] content. This approves that the added ionic liquid was indeed added into cross-linked PEG membranes.

4.1.3 FT-IR result of membranes with [Bmim][PF_6]

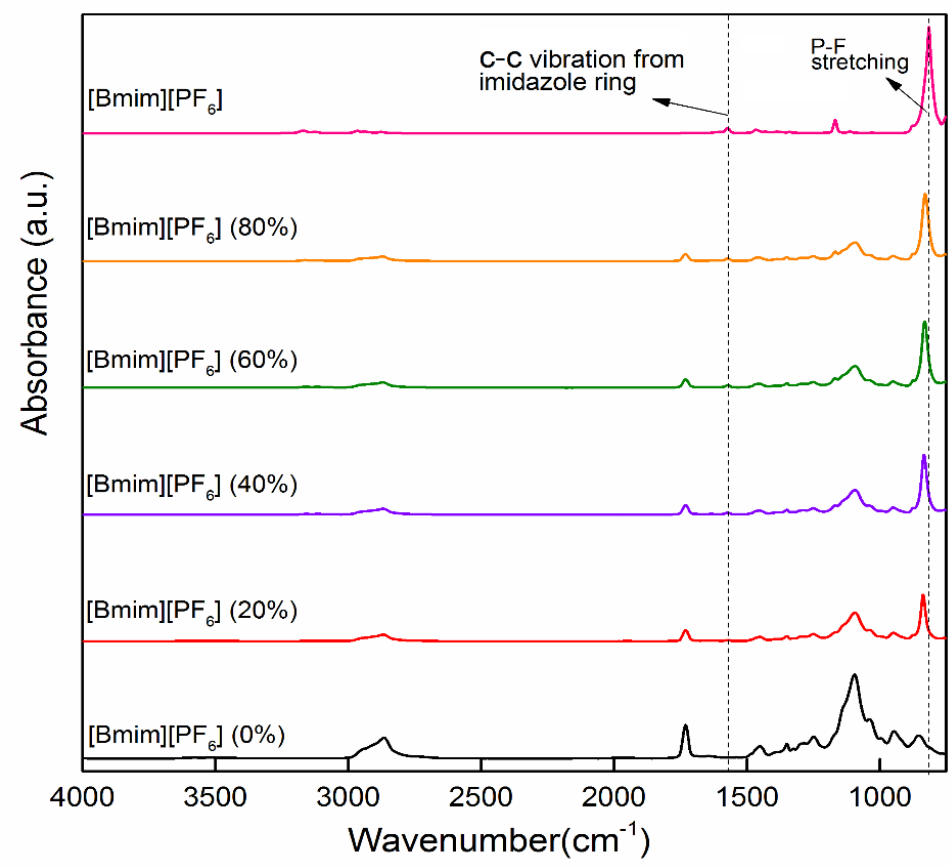

Figure 4.3 FT-IR result of PEGDA/[Bmim][PF_6] membrane with different [Bmim][PF_6] content

The FT-IR spectrums of the cross-linked PEGDA/TAEA membranes with different content of [Bmim][PF_6] are depicted in Fig. 4.3. For pure [Bmim][PF_6], the peak between 1550 to 1600 cm^{-1} is related to the C-C vibration of the imidazole ring and the peak positioned on 843 cm^{-1} is the consequence of P-F stretching in $[PF_6]^-$. First of all, comparing the spectrums of cross-linked PEGDA/TAEA membrane and composite membrane with the ionic liquid, no new peak can be observed which confirms that [Bmim][PF_6] takes no part in the cross-linking reactions. Furthermore, it is unexpected to observe the intensities of two characteristic peaks of [Bmim][PF_6] remaining the

same when the [Bmim][PF_6] content is increased from 40% to 80%. This phenomenon suggests that the cross-linked PEG matrix may have a certain limitation for the added [Bmim][PF_6], hence a large amount of [Bmim][PF_6] could not be added successfully into the matrix as expected.

4.1.4 FT-IR result of membrane with [Bmim][Tf_2N]

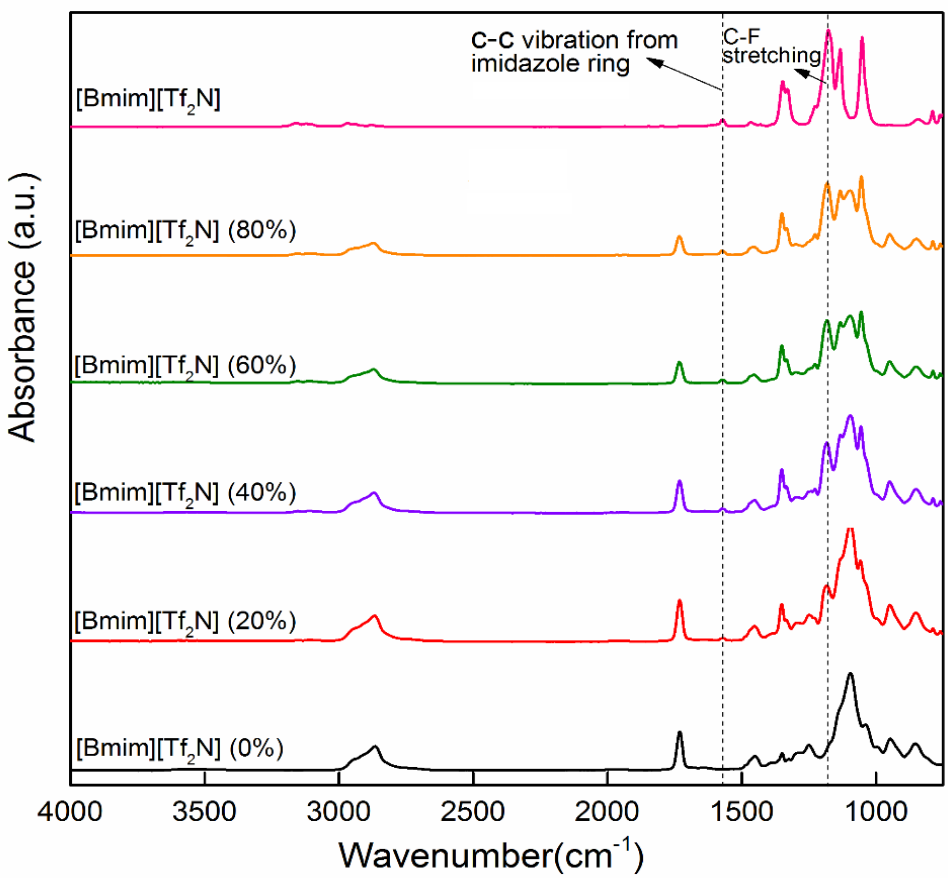

Figure 4.4 FT-IR result of PEGDA/[Bmim][Tf_2N] membrane with different [Bmim][Tf_2N] content

The FT-IR spectrum of the cross-linked PEGDA/TAEA membranes with different content of [Bmim][Tf_2N] are shown in Fig. 4.4. The peak between 1550 to 1600 cm^{-1} is corresponding to the C-C vibration of the imidazole ring and the peak positioned on

1200 cm^{-1} is the consequence of asymmetric C-F stretching in $[Tf_2N]^-$. Above all, comparing the spectrums of PEGDA/[Bmim][Tf_2N] composite membranes with the result of neat membrane matrix, no new peak related to new chemical bond appear. This is reasonable because [Bmim][Tf_2N] is supposed not to take part in the cross-linking reactions. Moreover, it is expected to observe the intensities of two characteristic peaks of ionic liquid increase with increasing the [Bmim][Tf_2N] content. This phenomenon confirms the addition of ionic liquid is indeed added inside of membrane matrix.

4.1.5 FT-IR result of membranes with [Bmim][TCM]

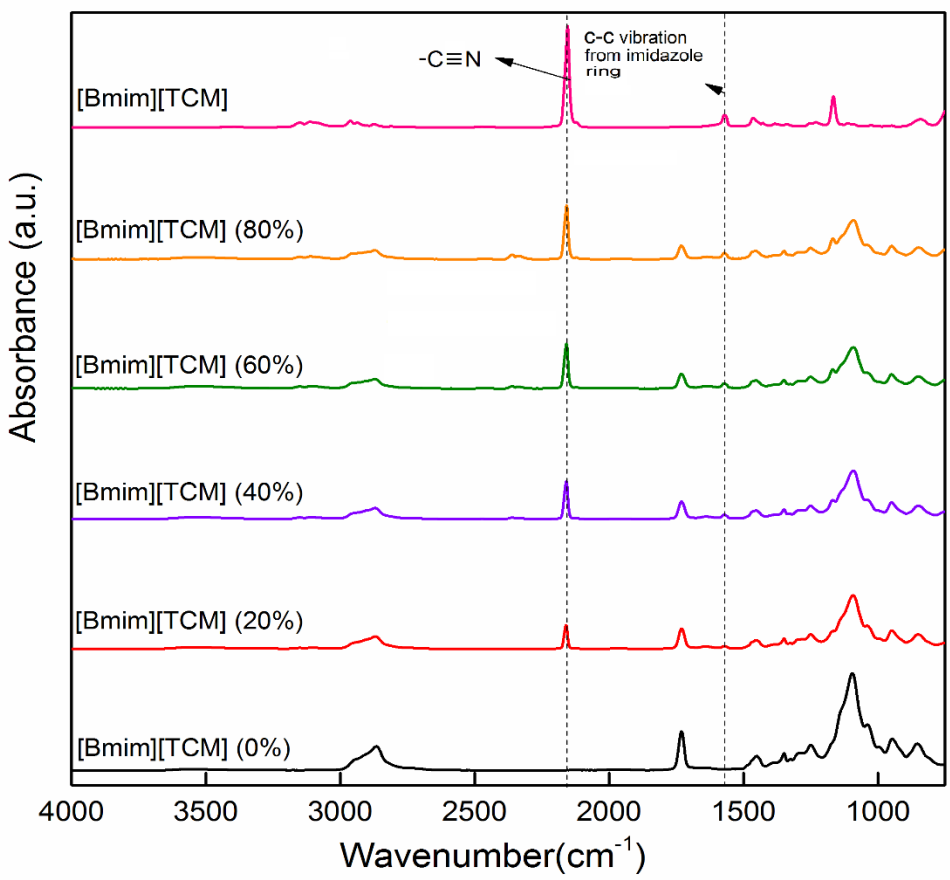

Figure 4.5 FT-IR result of PEGDA/[Bmim][TCM] membrane with different [Bmim][TCM] content

The FT-IR spectrums of the cross-linked PEGDA/TAEA membranes with different content of [Bmim][TCM] are presented in Fig. 4.5. The peak observed between 1550 and 1600 cm^{-1} are assigned to C-C vibration of the imidazole ring. The peak located at 2230 cm^{-1} is identified as C≡N bond from $[TCM]^-$. First of all, by comparing the spectrums of membranes with and without [Bmim][TCM], we can conclude that [Bmim][TCM] does not involve in the cross-linking reaction since no new peak related to new chemical bond occurs. Furthermore, as shown in the figure, the intensities of both characteristic peaks of [Bmim][TCM] increase with increasing content of ionic liquid. This observation helps us to conclude that the incorporation of [Bmim][TCM] is successful.

4.2 TGA results

The thermal stability of PEGDA/IL composite membranes is investigated by thermogravimetric analysis. All the membrane samples were tested from 30 to 700 ºC at a heating rate of 10 ºC /min in a N_2 atmosphere. The decomposition behaviors of four kinds of composite membranes are analyzed and discussed.

4.2.1 TGA result of membranes with [Bmim][BF_4]

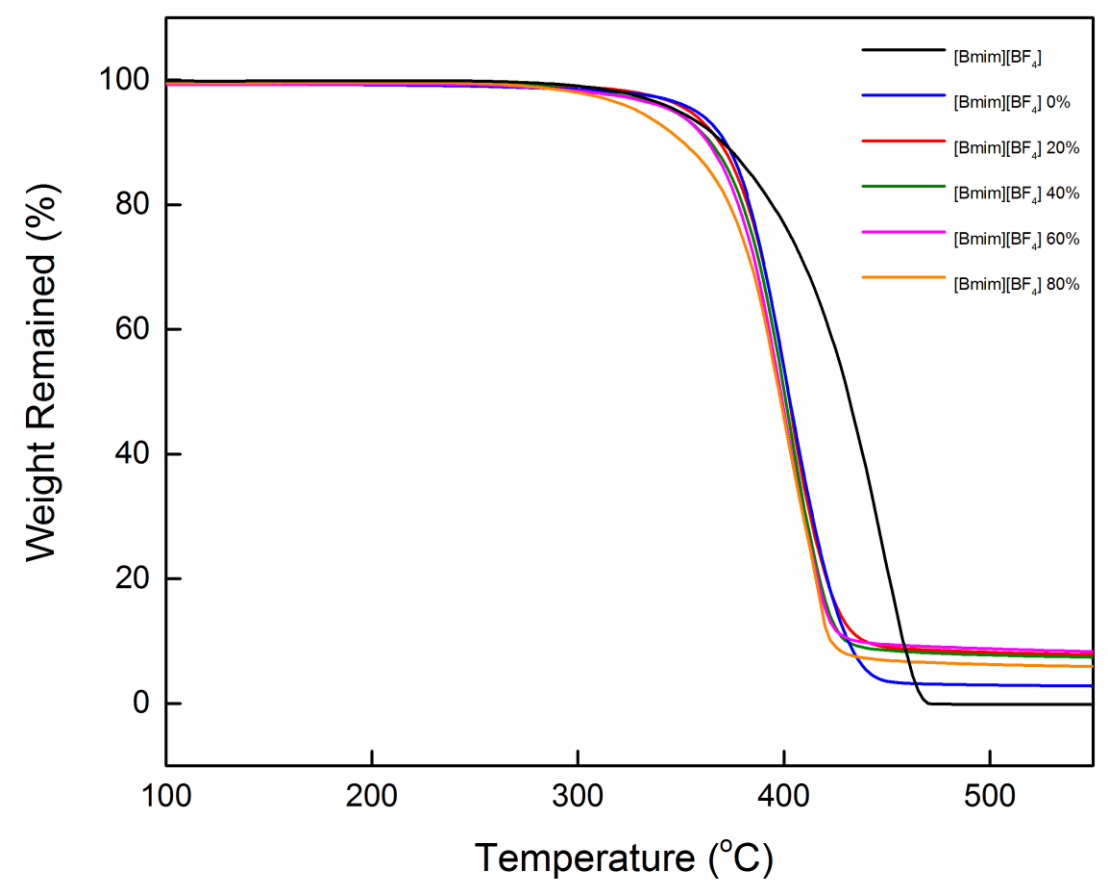

Figure 4.6 TGA result of PEGDA/[Bmim][BF_4] membrane with different [Bmim][BF_4] content

Figure 4.6 presents the TGA results of the [Bmim][BF_4] and composite PEGDA/-[Bmim][BF_4] membranes with different ionic IL content. As shown in the figure above,

pure [Bmim][BF_4] has a wider decomposition temperature range which is from 360 to 460 ºC while cross-linked PEGDA polymer matrix decomposes from 390 to 450 ºC. Both materials have displayed one stage degradation behavior and the decomposition temperature ranges are overlapped. The decomposition curves of all [Bmim][BF_4] composite membranes are similar to the membrane matrix's, especially from 390 to 420ºC, as shown in Figure 4.6. Also, the initial decomposition temperature of the composite films decreases with increasing the ionic liquid content. The reason is that the initial decomposition temperature of the ionic liquid is lower than the membrane matrix.

4.2.2 TGA result of membranes with [Bmim][PF_6]

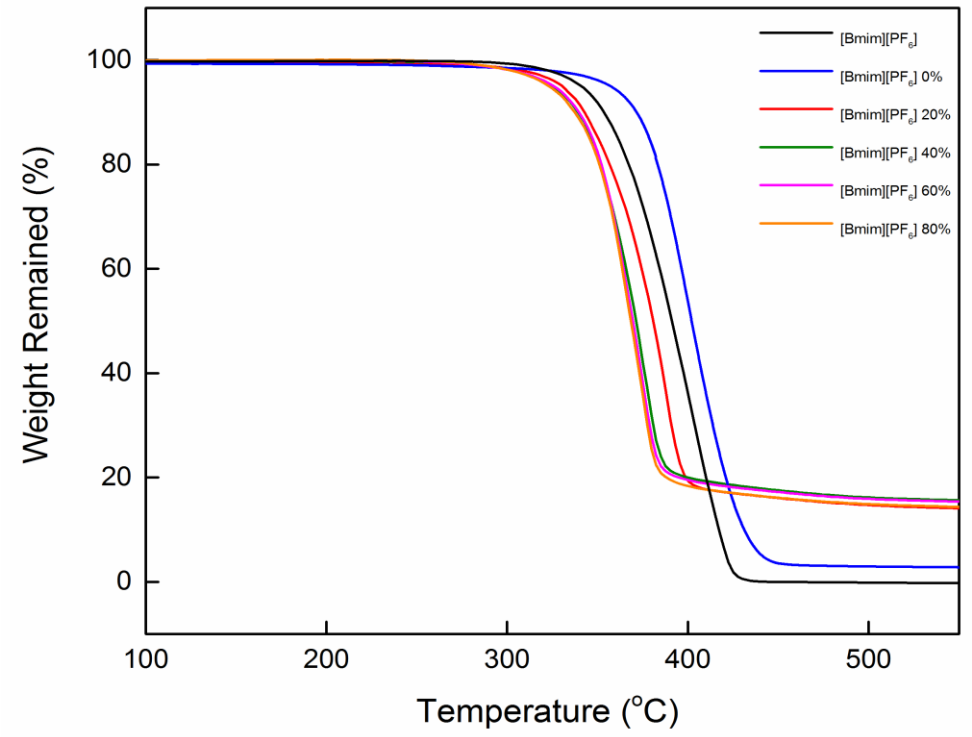

Figure 4.7 TGA result of PEGDA/[Bmim][PF_6] membrane with different [Bmim][PF_6] content

Figure 4.7 shows the TGA result of the [Bmim][PF_6] and cross-linked PEGDA/-[Bmim][PF_6] composite membranes with different ionic liquid content. First of all, all the samples have one-stage decomposition behavior. Pure [Bmim][PF_6] decomposes from 380 to 480 ^oC and the cross-linked PEGDA membrane matrix degraded from 390 to 450 ^oC. An overlap of the decomposition temperature range is observed. Secondly, as shown in the figure, all composite membranes show worse thermal stability than the parent: [Bmim][PF_6] and membrane matrix. The possible explanation for it is some interactions between [Bmim][PF_6] and membrane matrix undermine the thermal stability. Furthermore, it can be clearly observed the degradation curves of composite membranes with 40%, 60%, 80% of [Bmim][PF_6] are roughly the same. Combined with the FT-IR results of PEGDA/[Bmim][PF_6] membranes, we may speculate the actual content of ionic liquid in the composite membrane samples with 40%, 60%, 80% [Bmim][PF_6] probably is quite similar. Then, there may be unknown limitation of blending [Bmim][PF_6] into the composite membrane.

4.2.3 TGA result of membranes with [Bmim][Tf_2N]

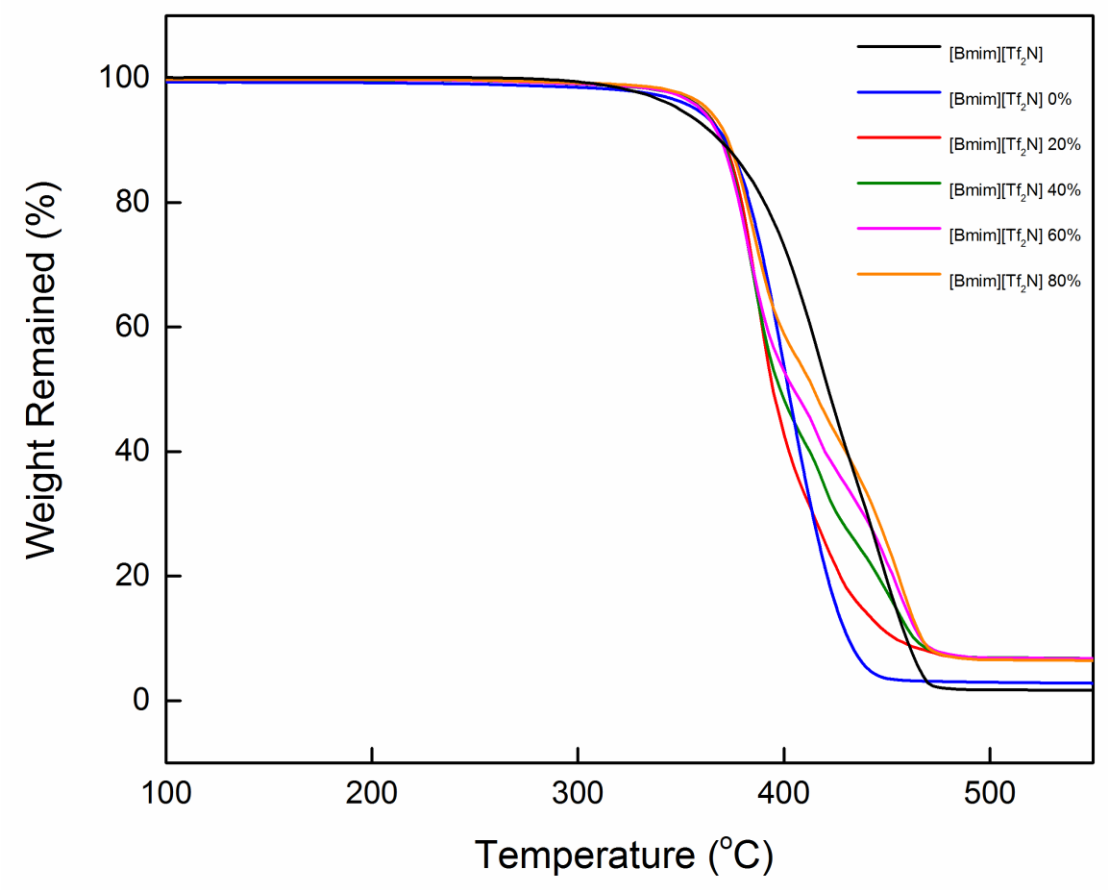

Figure 4.8 TGA result of PEGDA/[Bmim][Tf_2N] membrane with different [Bmim][Tf_2N] content

Figure 4.8 shows the TGA results of the [Bmim][Tf_2N] and cross-linked PEGDA/-[Bmim][Tf_2N] membranes with different [Bmim][Tf_2N] content. All the samples display one stage decomposition behavior. Pure [Bmim][Tf_2N] decomposes from 330 to 480 ^oC, while cross-linked PEGDA membrane matrix decomposes from 390 to 450 ^oC. Their decomposition temperature ranges are overlapped from 390 to 450 ^oC. The thermal stability of [Bmim][Tf_2N] is slightly better than membrane matrix. By comparing the slope of TGA curves, we can see the decomposition rate of polymer matrix is faster than [Bmim][Tf_2N]. The composite membranes display similar

decomposition behavior from 370 to 395 ºC. But from 395 to 450 ºC, as the content of [Bmim][Tf_2N] increases, the decomposition curve gets close to the curve of the pure [Bmim][Tf_2N], indicating the PEGDA/TAEA membrane matrix mainly decomposes at lower temperature from 370 to 395 ºC and the ionic liquid blended in the matrix mainly decomposes from 395 to 450 ºC.

4.2.4 TGA result of membranes with [Bmim][TCM]

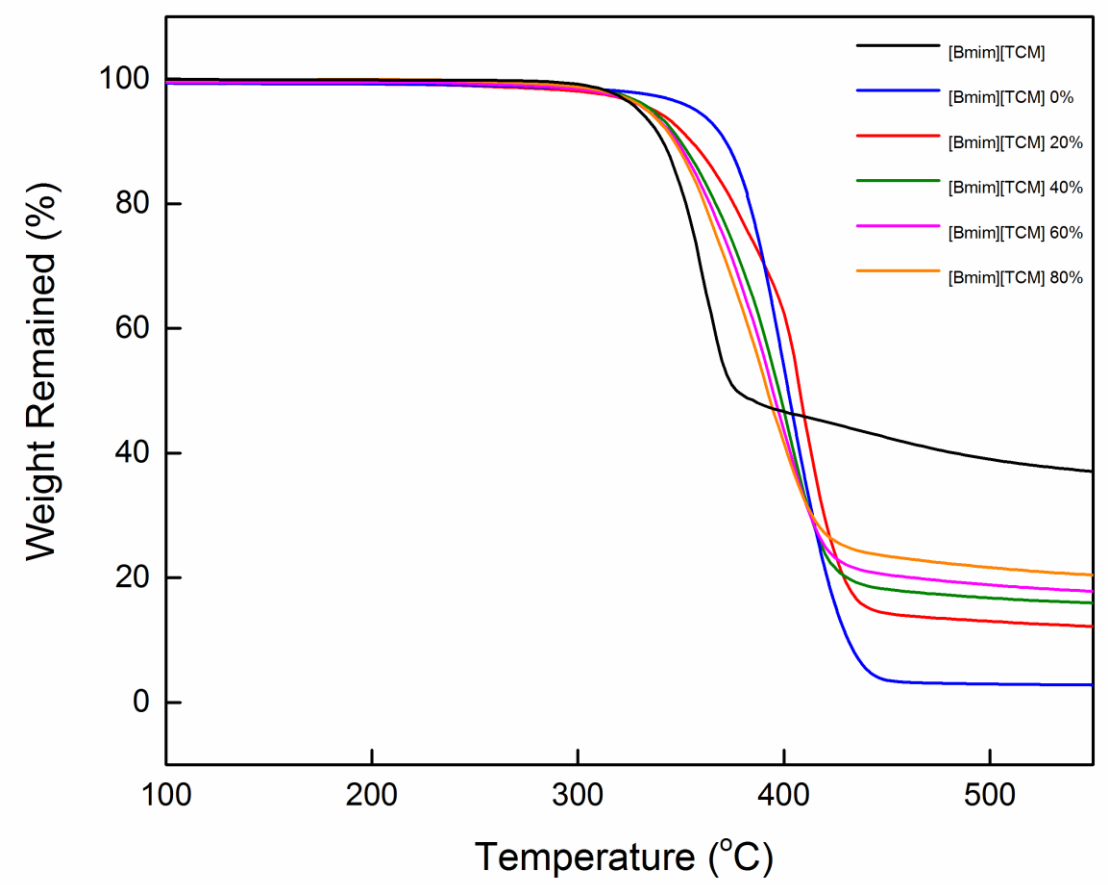

Figure 4.9 TGA result of PEGDA/[Bmim][TCM] membrane with different [Bmim][TCM] content

Figure 4.9 depicts the TGA results of the [Bmim][TCM] and composite PEGDA/-[Bmim][TCM] membranes with different IL content. For pure [Bmim][TCM], 55% of

the weight loss happen between 310 and 380 ºC, while 40% of the mass is left and staying stable after 550 ºC. Cross-linked PEGDA membrane matrix decomposes from 390 to 450 ºC. The decomposition temperature ranges of the two basic substances do not overlap, but they are quite close. This may explain why all composite membranes have one stage decomposition behavior. The TGA curves of d composite membranes with different IL content are between two pure components. With higher IL content, the decomposition curve of composite membrane gets closer to the curve of the pure [Bmim][TCM].

4.3 DSC results

Phase transition behaviors of composite PEGDA/IL membranes with different ionic liquid content are studied by differential scanning calorimetry test from -100 to 150 °C under N_2 atmosphere. The results are analyzed and discussed.

4.3.1 DSC result of membranes with [Bmim][BF_4]

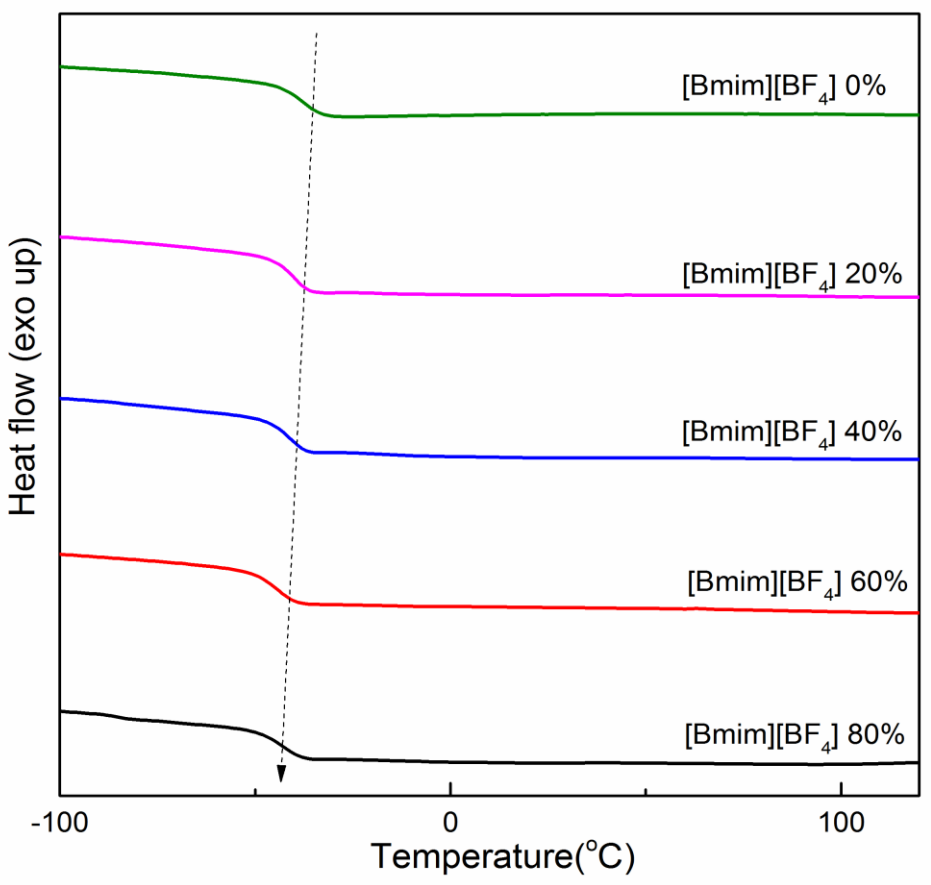

Figure 4.10 DSC result of PEGDA/[Bmim][BF_4] membrane with different [Bmim][BF_4] content

DSC results of PEGDA/[Bmim][BF_4] composite membranes are presented in Figure 4.10. All the composite membranes with different content of [Bmim][BF_4] have single glass transition behavior around -46 °C and there do not exist melting behavior. We can

conclude that all the composite membranes are in the rubbery state as well as the IL is well dispersed in the polymer matrix. It can be observed in the Figure 4.10 that as the [Bmim][BF_4] content increases, all T_g values slightly decreases from -44 ^oC to -48.3 ^oC. The decrease in the T_g suggest that the polymer chain mobility is improved and may indicate the FFV is enhanced. This may give some positive effect on the gas transportation effect.

4.3.2 DSC result of membranes with [Bmim][PF_6]

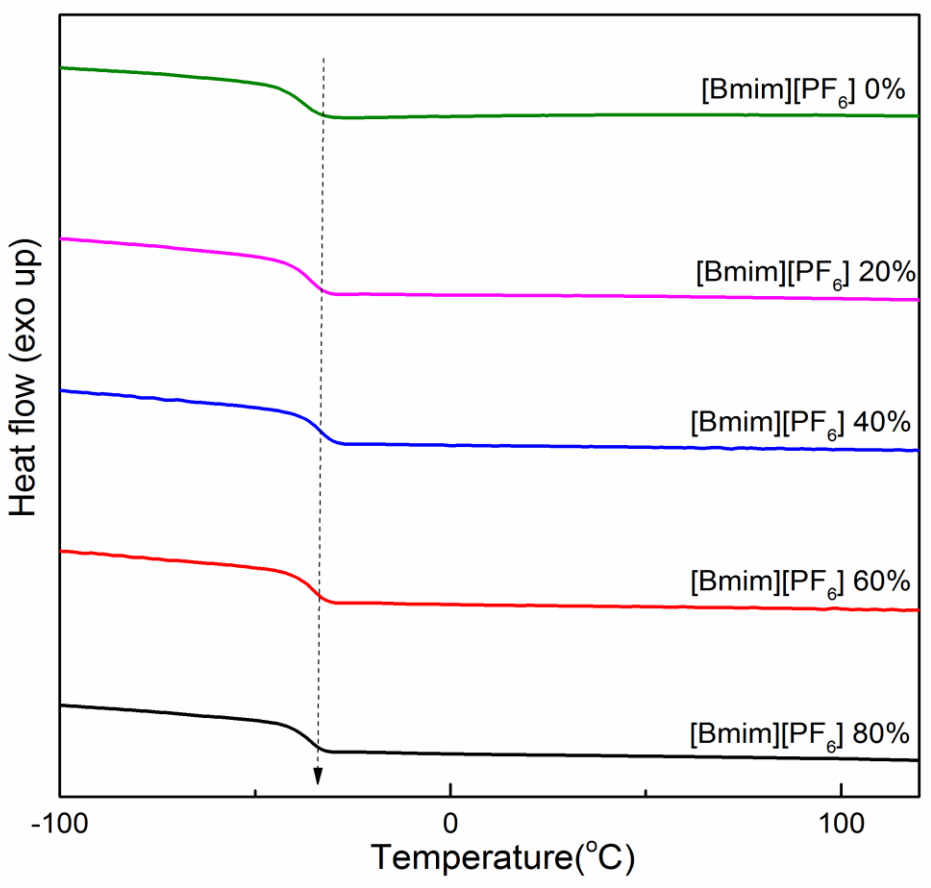

Figure 4.11 DSC result of PEGDA/[Bmim][PF_6] membrane with different [Bmim][PF_6] content

DSC results of PEGDA/[Bmim][PF_6] composite membranes are presented in Figure

4.11. Firstly, all membrane samples have single glass transition behavior around -45 ºC, indicating all composite membrane samples are in the rubbery state at room temperature. Secondly, no melting behavior can be observed in all composite membranes. Based on this result, we can conclude that the IL is well dispersed in the polymer matrix because IL zone presented in polymer matrix is not large enough to exhibit crystal melting behavior. As shown in the figure above, when the [Bmim][PF_6] content increases, the T_g do not have a significant change.

4.3.3 DSC result of membranes with [Bmim][Tf_2N]

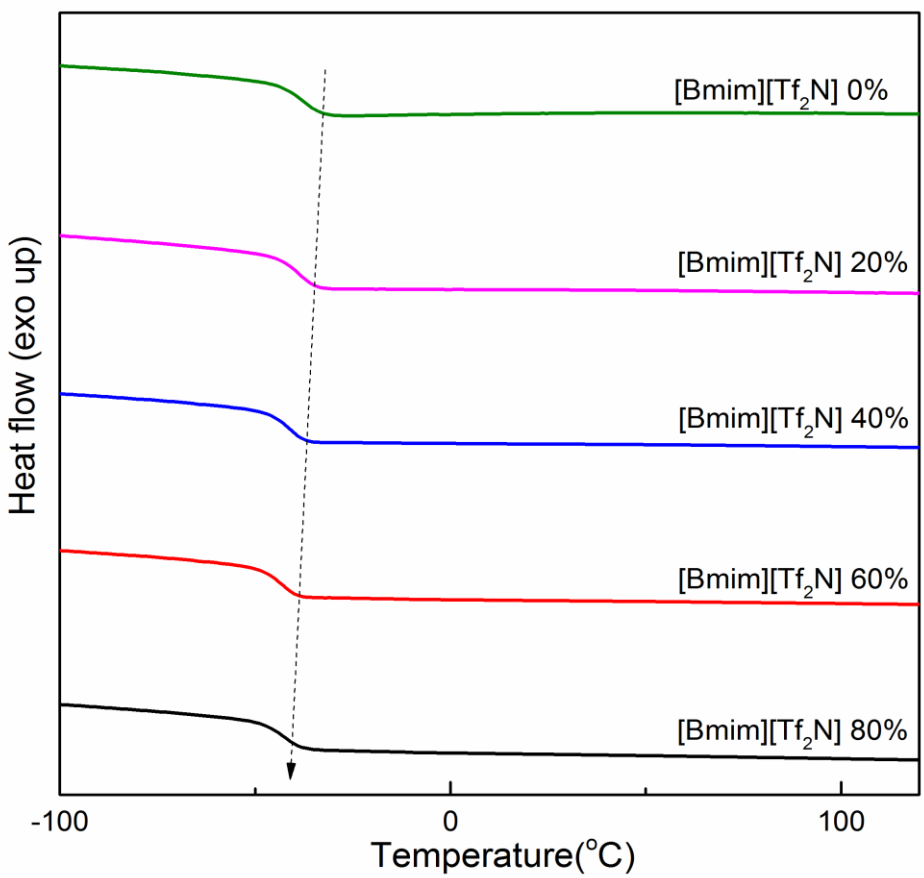

Figure 4.12 DSC result of PEGDA/[Bmim][Tf_2N] membrane with different [Bmim][Tf_2N] content

DSC results of PEGDA/[Bmim][Tf_2N] composite membranes are depicted in Figure 4.12. All the hybrid membranes with different [Bmim][Tf_2N] content display glass transition temperature around -44 ^oC to -48 ^oC. So, we can conclude all the composite membranes are in the rubbery state at the testing temperature of 24 ^oC. Moreover, no melting transitions are observed in the DSC results. We can confirm the IL is well dispersed in the polymer matrix and strongly associated with the polymer chains, since the bulk IL presented in domains is not large enough to exhibit crystal melting behavior (Kusuma et al., 2018). The glass transition temperature declines slightly from -44 to -48 ^oC when increasing the [Bmim][Tf_2N] content from 0% to 80%. It is due to the addition of free ionic liquid which increases the polymer chain mobility. Since the chain mobility strongly affects the transportation of gas through the polymeric membrane, a growth of the gas permeability can be expected with the increment of [Bmim][Tf_2N] content.

4.3.4 DSC result of membranes with [Bmim][TCM]

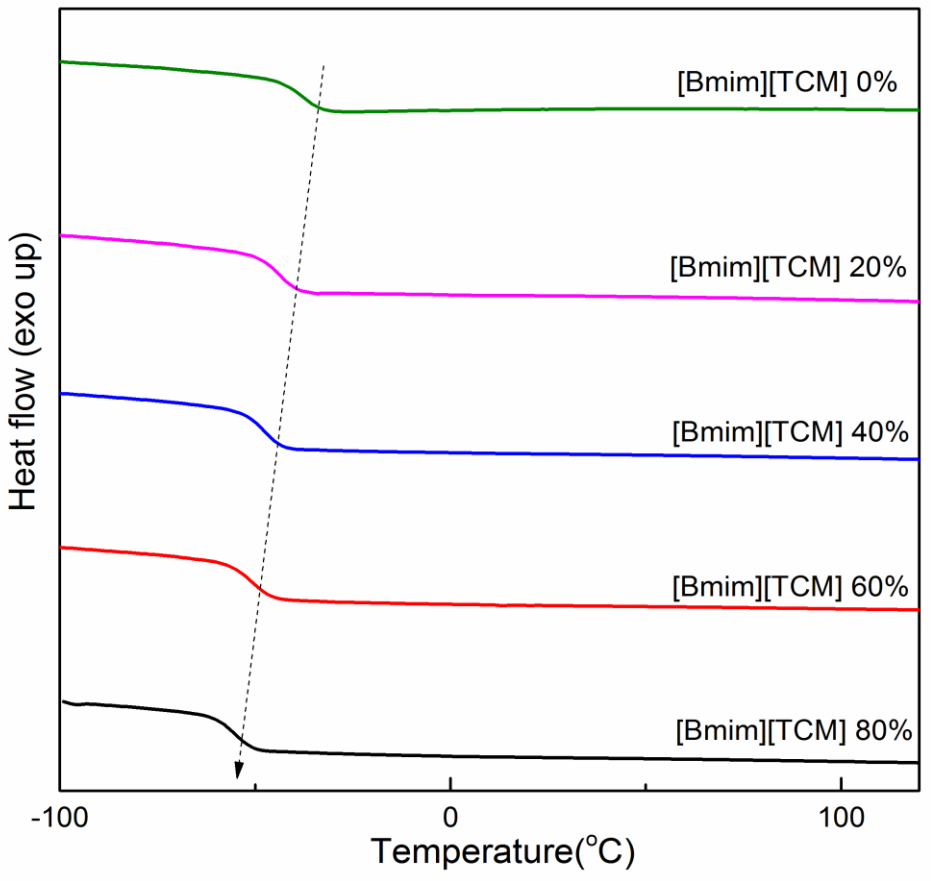

Figure 4.13 DSC result of PEGDA/[Bmim][TCM] membrane with different [Bmim][TCM] content

DSC results of PEGDA/[Bmim][TCM] composite membranes are presented in Figure 4.13. All the composite membranes with different amount of [Bmim][TCM] perform glass transition temperatures around -44 to -51 ºC. So, we can confirm that all the composite membranes are in the rubbery state at the room temperature of 24 ºC. An obvious reduction in the glass transition temperature from -44 to -51 ºC can be observed when the [Bmim][TCM] content is increased from 0% to 80%. It is because the incorporation of free ionic liquid enhances the chain mobility. We may expect an improvement on the gas transportation performance.

4.4 XRD results

A

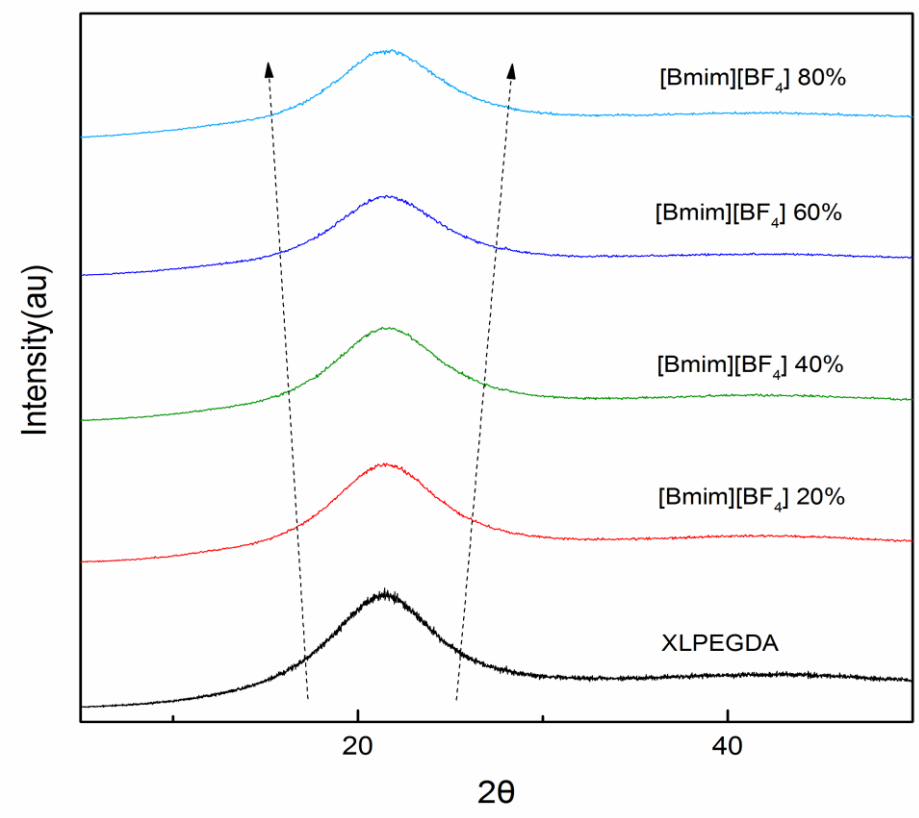

B

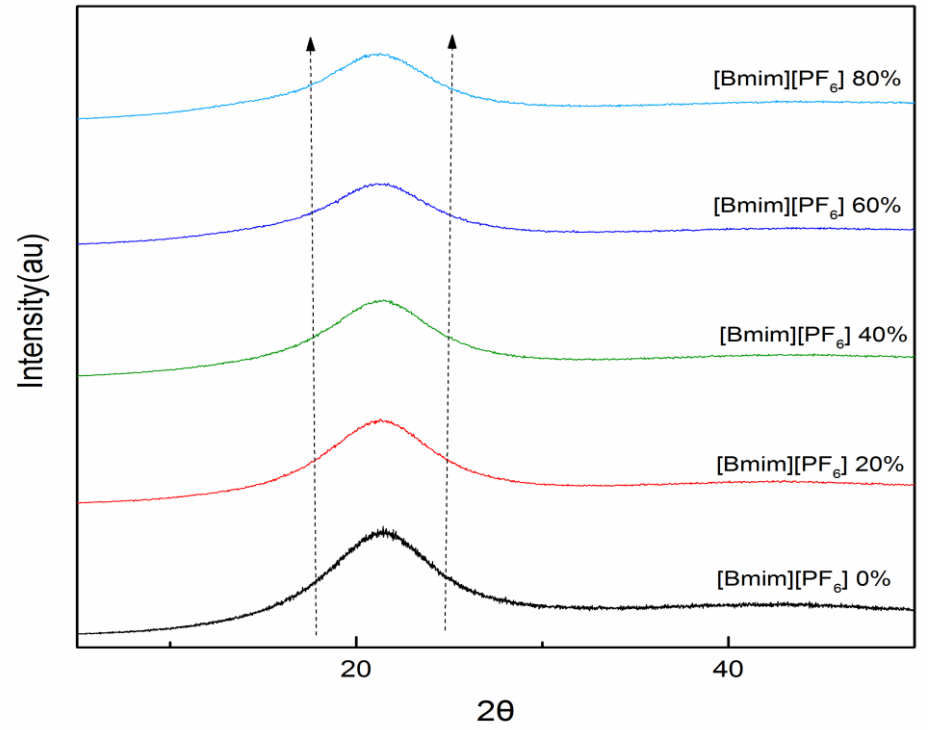

C

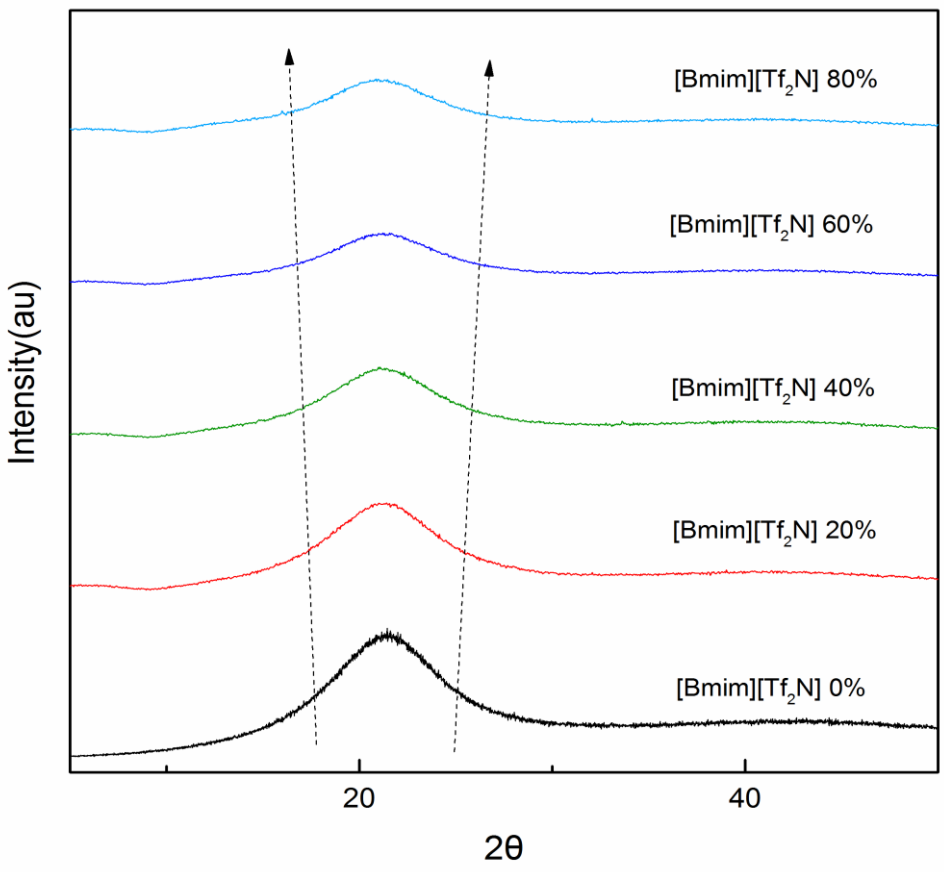

D

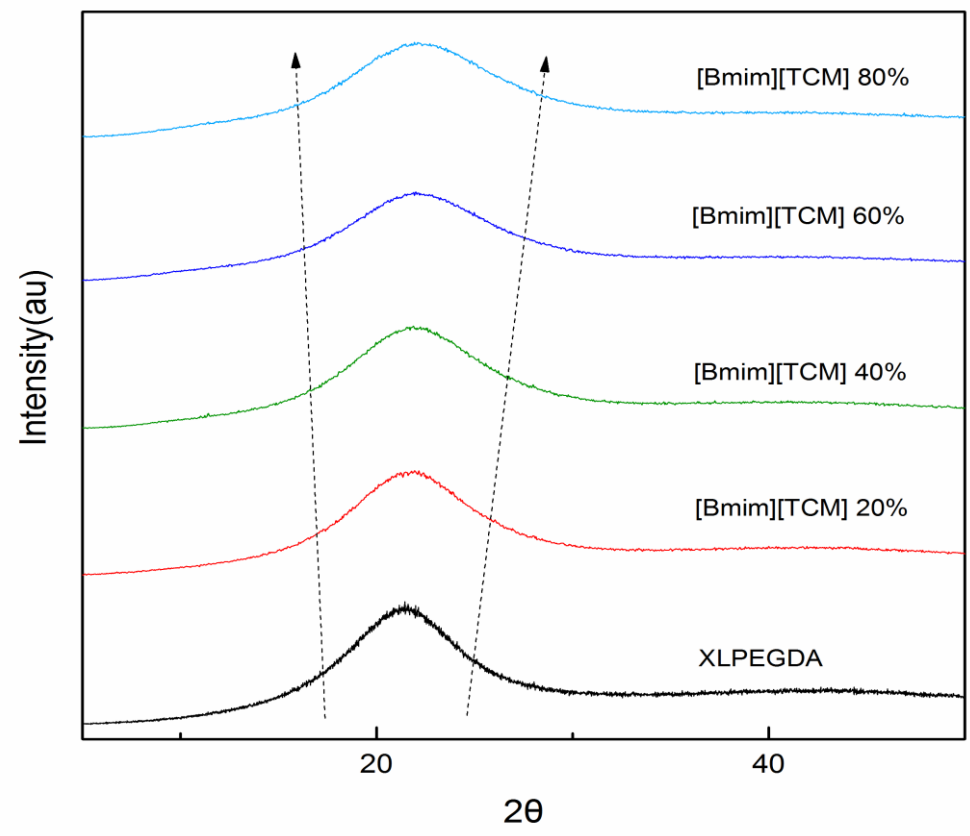

Figure 4.14 XRD results of PEGDA/IL membranes with different IL content

XRD tests were made for all the PEGDA/IL composite membranes to study their crystallization. Figure 4.14 presents the XRD results of four different PEGDA/IL composite membranes with different ionic liquid content. For all the membranes, from the figure, it can be observed that all the membranes have a single broad peak around 21°, suggesting all resultant membranes are in the amorphous state.

Moreover, for each kind of membranes, by the addition of ionic liquid, the peak becomes broader than the one of neat cross-linked PEGDA membrane. The intensity of the peak decreases as the content of ionic liquid increases. This result points out the crystallization of the membranes is decreased by incorporating simply with ionic liquid. This conclusion is consistent with the conclusion drawn from DSC results.

To sum up, according to the results, it can be confirmed that all the membranes at room temperature are amorphous and high trend of crystallization of PEO-based materials is suppressed.

4.5 Water uptake results

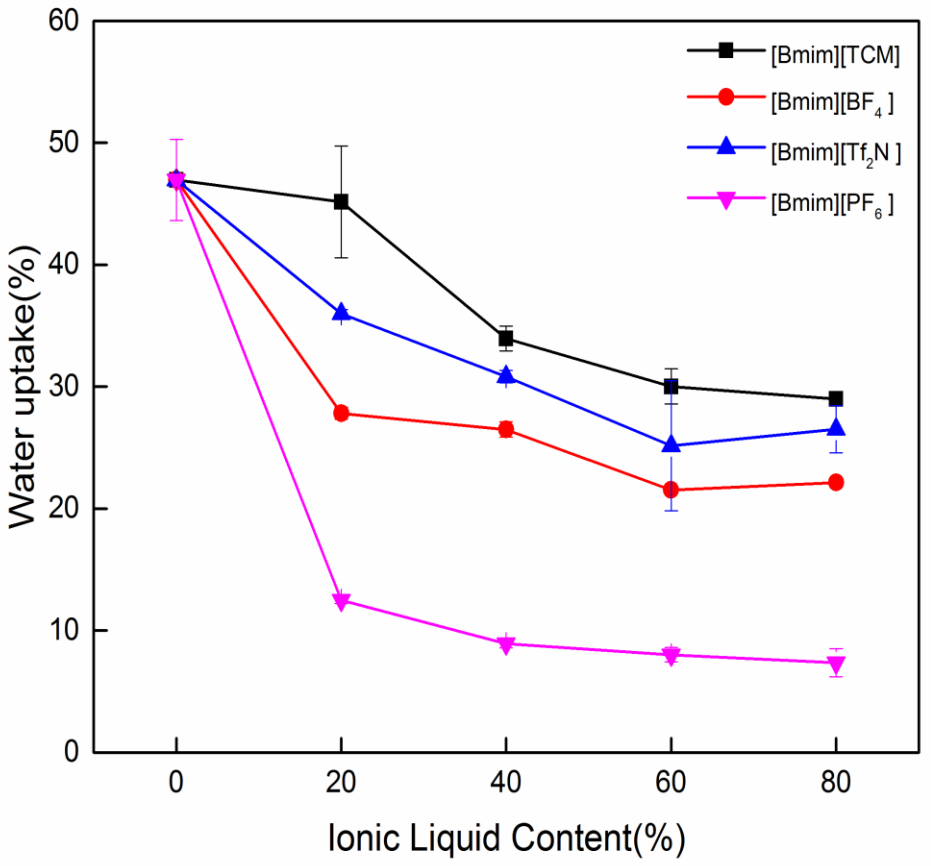

Figure 4.15 Water uptake results of PEGDA/IL membrane with different IL content

The hydrophilicity of cross-linked PEGDA membrane matrix and PEGDA/IL composite membranes at various IL content are investigated by water uptake experiment. It can be observed from the Figure 4.15, the water uptake in all PEGDA/IL composite membranes is lower than that of the neat cross-linked PEGDA membrane. As the ILs content in the composite membrane increases, the water uptake decreases more, that means the hydrophilicity of the membrane is reduced. This is expected since these four-ionic liquids are more hydrophobic comparing with the PEG-based membrane. The more ILs is added, the less hydrophilicity the membrane has. As shown in the figure, the hydrophilicity of composite membranes blended with different IL

increase as follow: PEGDA/[Bmim][PF_6] membranes < PEGDA/[Bmim][BF_4] membranes < PEGDA/ [Bmim][Tf_2N] membranes < PEGDA/Bmim][TCM] membranes. This is not expected because of these ionic liquids, [Bmim][PF_6] and [Bmim][BF_4] are more hydrophilic than [Bmim][Tf_2N]. The reason should be further investigated.

4.6 Single gas results

The effect of the adding four ionic liquids varying in content on gas separation performance is investigated. The gas permeabilities (CO_2 and N_2) are obtained and ideal selectivity based on Equ. 2.2 are calculated. According to the solution-diffusion model mentioned in Chapter 2, gas permeability is determined by both diffusivity and solubility. To find out the influence of ILs on gas transport properties, the diffusivity and solubility are also calculated based on time-lag method.

4.6.1 Single gas result of membranes with [Bmim][BF_4]

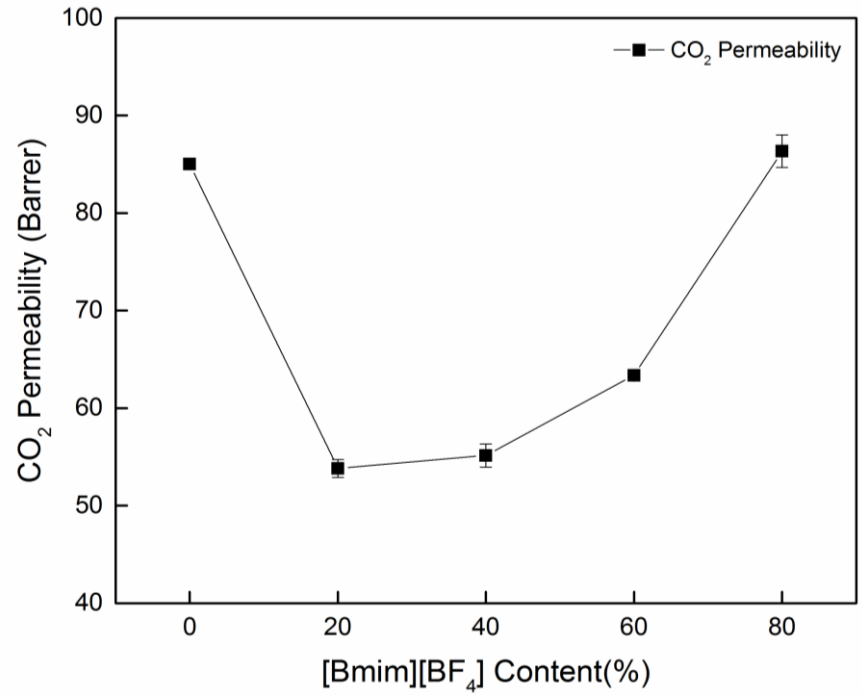

Figure 4.16 CO_2 Permeability of PEGDA/[Bmim][BF_4] membrane with different [Bmim][BF_4] content

The effect of [Bmim][BF_4] content on gas separation performance is investigated. Figure 4.15 and 4.16 present the CO_2 permeability and ideal CO_2/N_2 selectivity at room

temperature as a function of the [Bmim][BF_4] content, respectively. A drastic decrease in permeability is observed when the content of ionic liquid increases from 0% to 20%. While it increases from 52 to 82 Barrer with the increasing IL content up to 80%. For ideal CO_2/N_2 selectivity, it declines from 63.5 to 42.

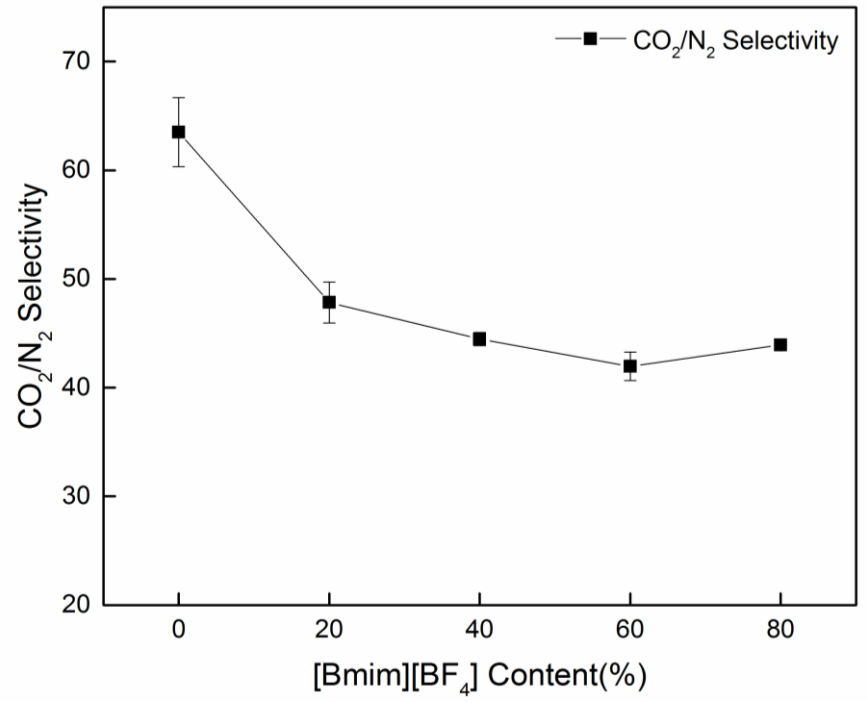

Figure 4.17 CO_2 /N_2 Selectivity of PEGDA/[Bmim][BF_4] membrane with different [Bmim][BF_4] content

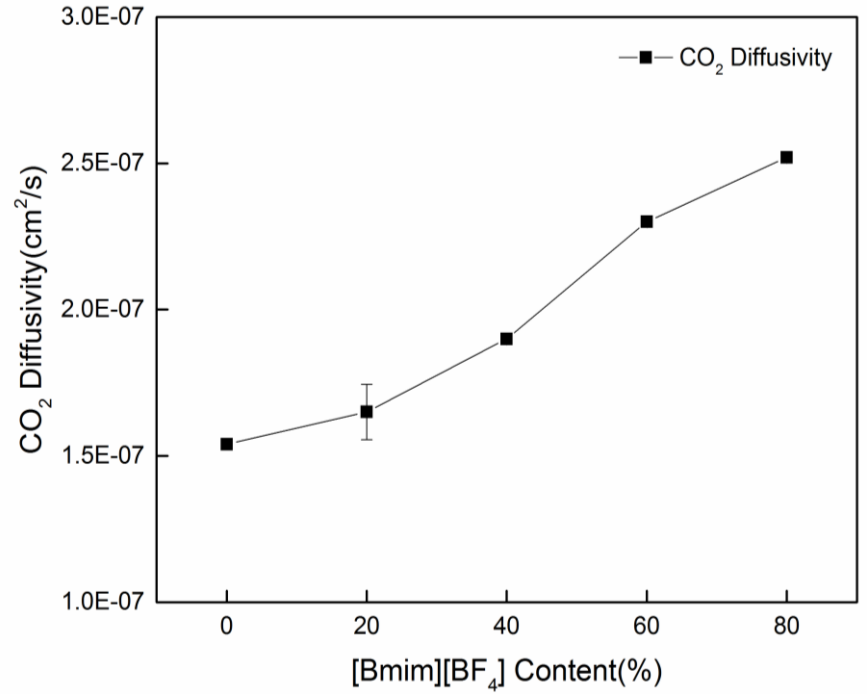

Figure 4.18 CO_2 Diffusivity of PEGDA/[Bmim][BF_4] membrane with different [Bmim][BF_4] content

Figure 4.17 and 4.18 show CO_2 diffusivity and CO_2 solubility of PEGDA/[Bmim][BF_4] composite membranes as a function of the ionic liquid content. The CO_2 diffusivity increases monotonically with [Bmim][BF_4] content. This is the result of plasticization effect which improves the polymer chain flexibility and increases the FFV of the polymer matrix. In contrast, the CO_2 solubility decreases until the content reaches 20% and then keeps constant regardless of the increment of ionic liquid content. This is because the PEGDA membrane matrix is more CO_2-philic than [Bmim][BF_4]. Since the permeability is the product of solubility and diffusivity, it is reasonable that CO_2 permeability decreases when ionic liquid content is lower than 20%, while it grows at higher content.

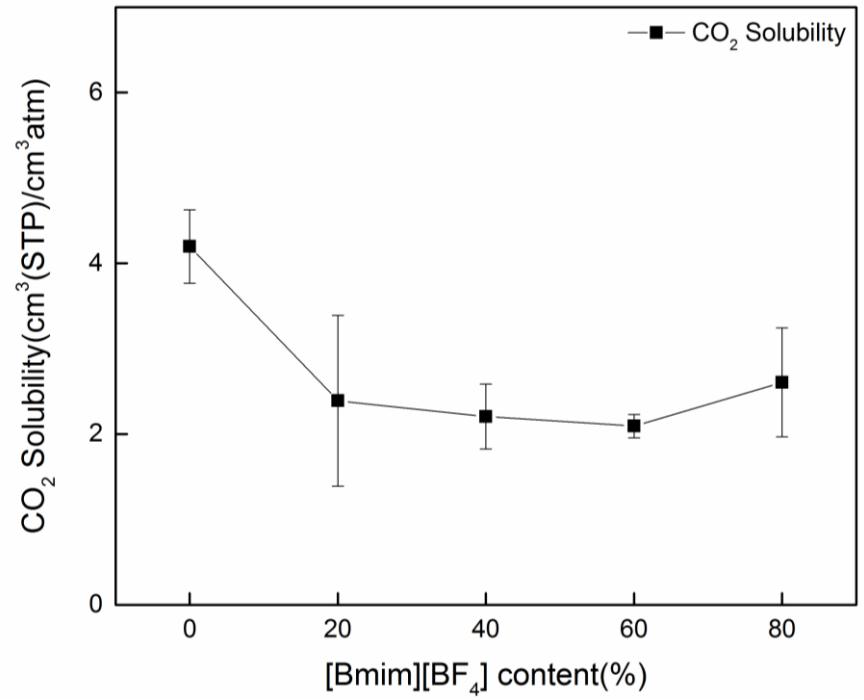

Figure 4.19 CO_2 Solubility of PEGDA/[Bmim][BF_4] membrane with different [Bmim][BF_4] content

4.6.2 Single gas result of membranes with [Bmim][PF_6]

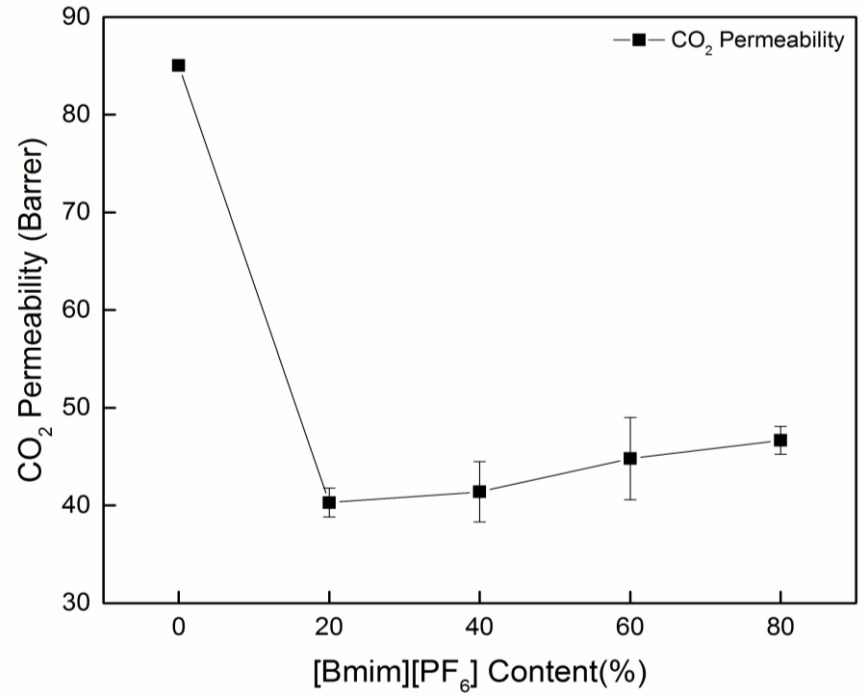

Figure 4.20 CO_2 Permeability of PEGDA/[Bmim][PF_6] membrane with different [Bmim][PF_6] content

The effect of the addition of [Bmim][PF_6] on gas separation performance is first investigated. Figure 4.20 and 4.21 present the CO_2 permeability and ideal CO_2/N_2 selectivity at room temperature as a function of the [Bmim][PF_6] content, respectively. With the increment of [Bmim][PF_6] content, it is observed that a significant decrease in permeability from 85 to 40 Barrer at a low loading of [Bmim][PF_6] (20%), followed a slight increase from 40 to 45 Barrer. The ideal selectivity decreases monotonously from 63.5 to 27. To evaluate the reason responsible for the CO_2 permeability's change, diffusivity and solubility are calculated and discussed below.

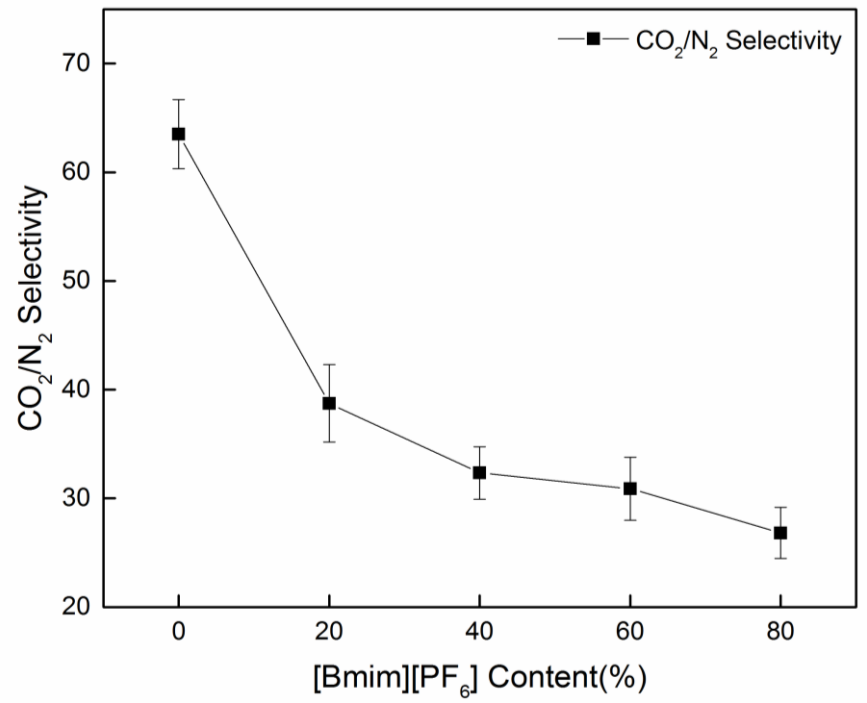

Figure 4.21 CO_2 /N2 Selectivity of PEGDA/[Bmim][PF_6] membrane with different [Bmim][PF_6] content

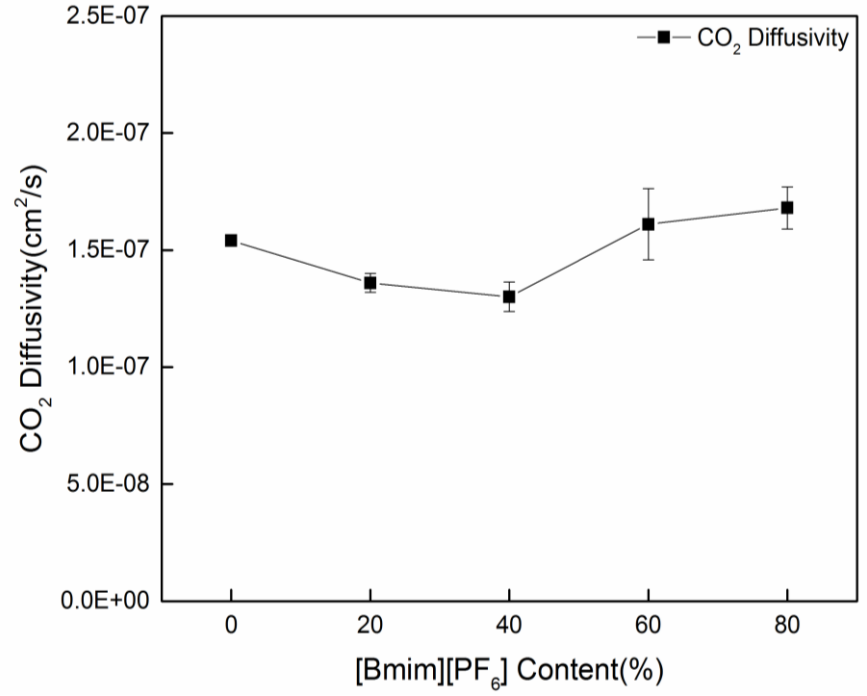

Figure 4.22 CO_2 Diffusivity of PEGDA/[Bmim][PF_6] membrane with different [Bmim][PF_6] content

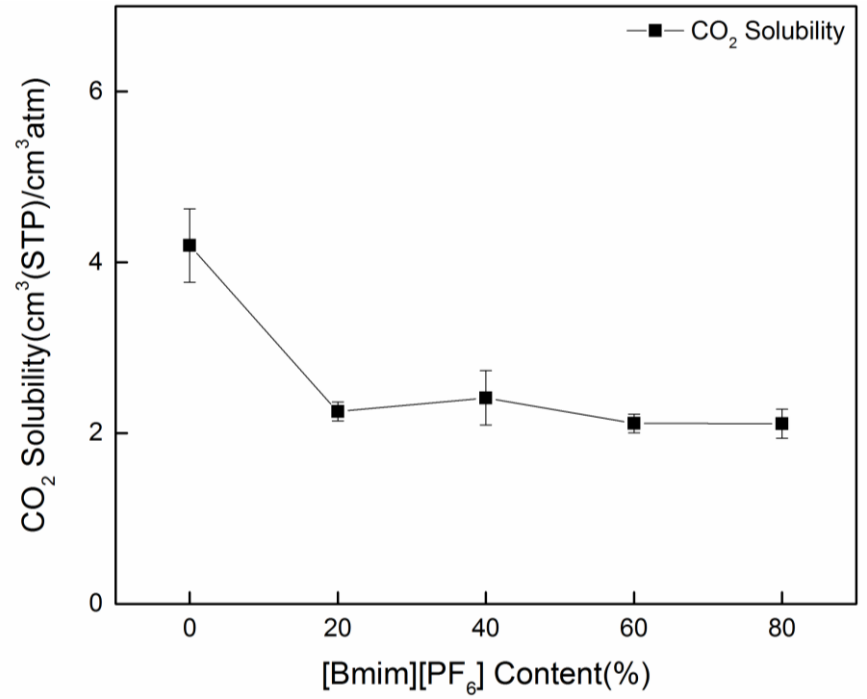

Figure 4.23 CO_2 Solubility of PEGDA/[Bmim][PF_6] membrane with different [Bmim][PF_6] content

Figure 4.22 and 4.23 show CO_2 diffusivity and CO_2 solubility of PEGDA/[Bmim][PF_6] membranes as a function of the ionic liquid content, respectively. As plotted in figure 4.18, when the ionic liquid content is increased from 0% to 40%, the CO_2 diffusivity slightly decreases from 1.54 to 1.30 × 10^{-7} cm^2/s and then increases to 1.68× 10^{-7} cm^2/s with a further addition of [Bmim][PF_6] to 80%. The slight decrease of diffusivity at the low ILs loading may be because the low amount of IL occupies the original free volume of polymer matrix (Kanehashi et al., 2013). After that, with continuingly adding [Bmim][PF_6], the chain mobility is improved and leads to an increment of diffusivity. Unlike CO_2 diffusivity, with increasing the ionic liquid content to 20%, the CO_2 solubility declines significantly from 4.2 to 2.1 cm^3(STP)/cm^3atm. This is because in general, comparing to the PEG-based material, the physical-absorption ILs, such as [Bmim][PF_6], have lower affinity to CO_2. The further incorporation does not change the CO_2 solubility anymore. Therefore, the rapid decrease in the CO_2 permeability with 20% [Bmim][PF_6] addition could be mainly corresponding to the sharp reduction of the gas solubility.

4.6.3 Single gas result of membranes with [Bmim][Tf_2N]

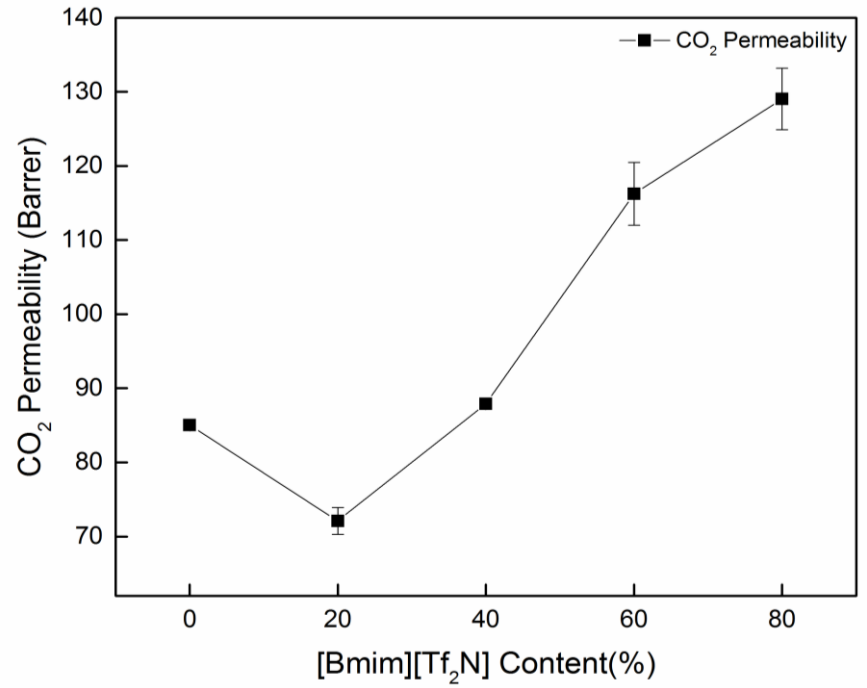

Figure 4.24 CO_2 Permeability of PEGDA/[Bmim][Tf_2N] membrane with different [Bmim][Tf_2N] content

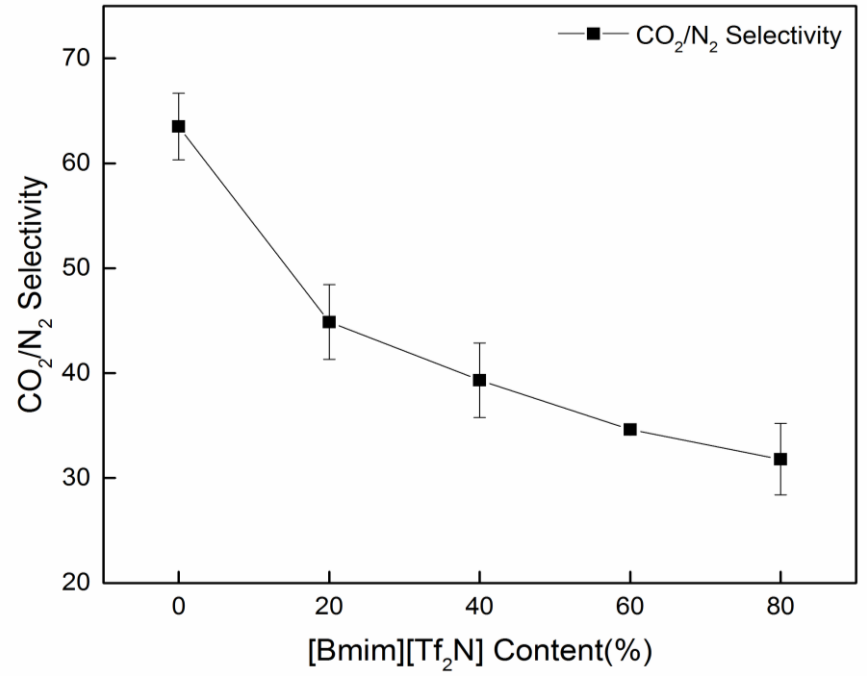

Figure 4.25 CO_2 /N2 Selectivity of PEGDA/[Bmim][Tf_2N] membrane with different [Bmim][Tf_2N] content

The effect of [Bmim][Tf_2N] content on gas separation performance is investigated. Figure 4.24 and 4.25 present the single gas permeability and ideal selectivity at room temperature as a function of the [Bmim][Tf_2N] content, respectively. With increasing the content of ionic liquid from 0% to 20%, the CO_2 permeability declines from 85 to 71 Barrer, and after, it increases to 130 Barrer with raising the ionic liquid content to 80%. Meanwhile, the ideal CO_2/N_2 selectivity decreases from 63.5 to 32.

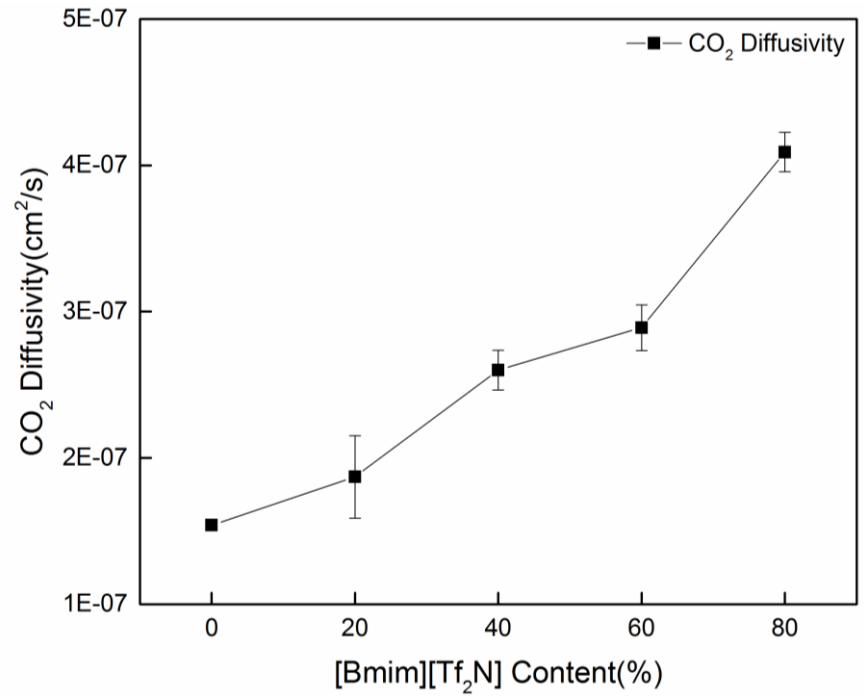

Figure 4.26 CO_2 Diffusivity of PEGDA/[Bmim][BF_4] membrane with different [Bmim][BF_4] content

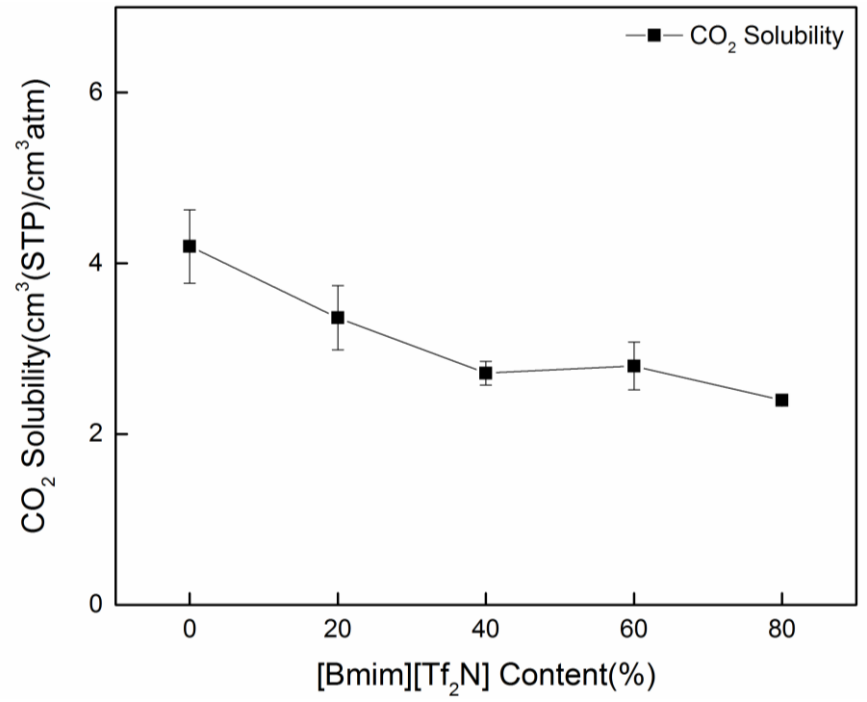

Figure 4.27 CO_2 Solubility of PEGDA/[Bmim][Tf_2N] membrane with different [Bmim][Tf_2N] content

Figure 4.26 and 4.27 show CO_2 solubility and CO_2 diffusivity of composite PEGDA/[Bmim][Tf_2N] membranes as a function of the ionic liquid content. With increasing ionic liquid content, CO_2 diffusivity increases sharply from 1.5 to 4.1×10^{-7} cm^2/s while the CO_2 solubility declines from 4.1 to 2.3 $cm^3(STP)/cm^3atm$. The addition of ionic liquid as plasticizers leading to more flexible chains and higher free volume in membranes resulting in the improvement of the CO_2 diffusivity. The decrease of solubility may be because the PEG polymer chains have higher CO_2 affinity than [Bmim][Tf_2N]. When ionic liquid content is < 40%, the CO_2 permeability is controlled by both diffusivity and solubility. It is a result of balance between decreased solubility and increased diffusivity. When ionic liquid content is > 40%, the change of CO_2 permeability is mainly caused by the change of diffusivity.

4.6.4 Single gas result of membranes with [Bmim][TCM]

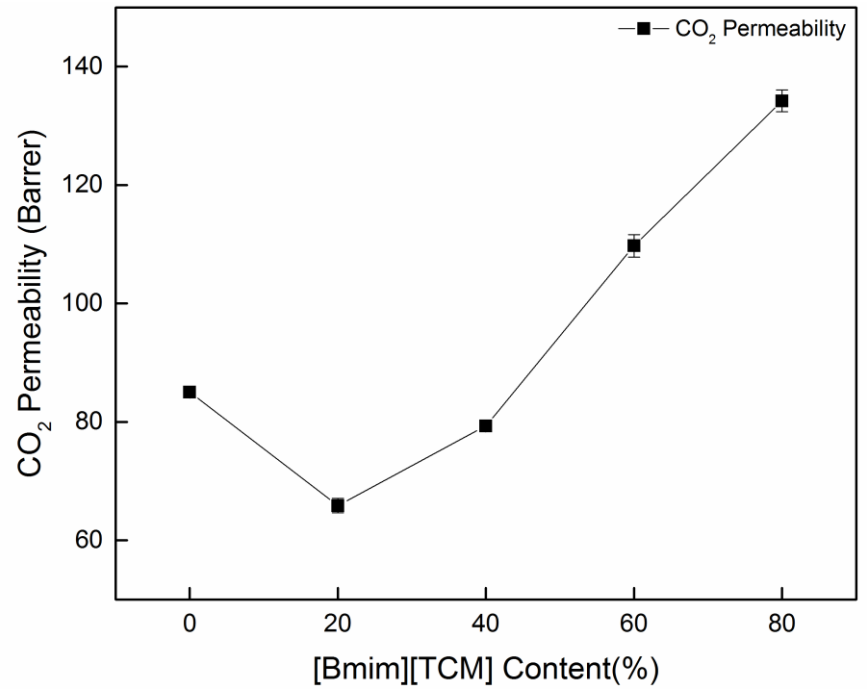

Figure 4.28 CO_2 Permeability of PEGDA/[Bmim][TCM] membrane with different [Bmim][TCM] content

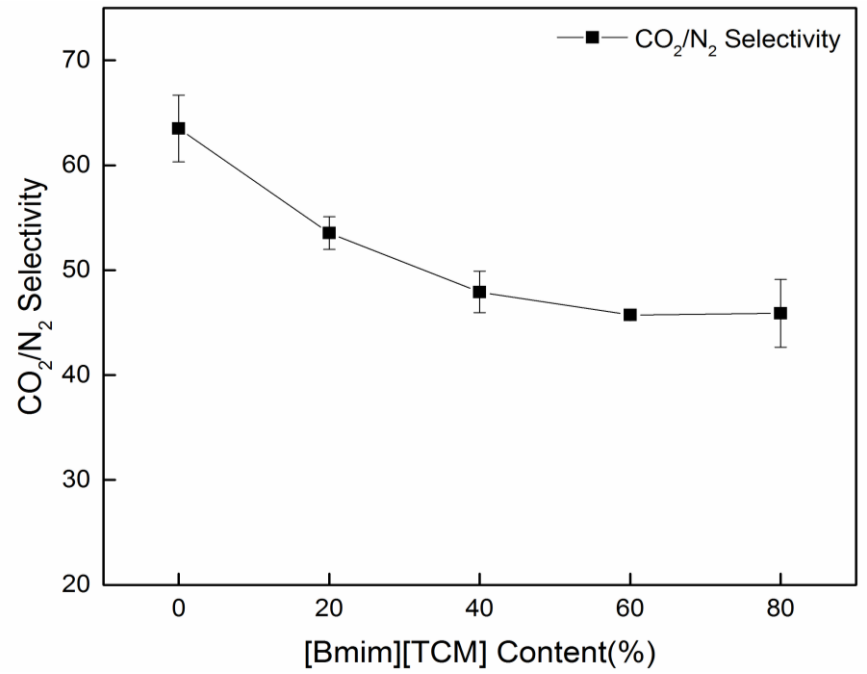

Figure 4.29 CO_2 /N2 Selectivity of PEGDA/[Bmim][TCM] membrane with different [Bmim][TCM] content

The effect of [Bmim][TCM] content on gas separation performance is investigated. Figure 4.28 and 4.29 present the single gas permeability and ideal CO_2/N_2 selectivity at room temperature as a function of the [Bmim][TCM] content, respectively. It can be seen when increasing the IL content from 0% to 20%, the CO_2 permeability decreases from 85 to 62 Barrer, and then with a further addition of IL to 80%, the CO_2 permeability increases to 138 Barrer. Moreover, the ideal selectivity decreases monotonously from 63 to 45.

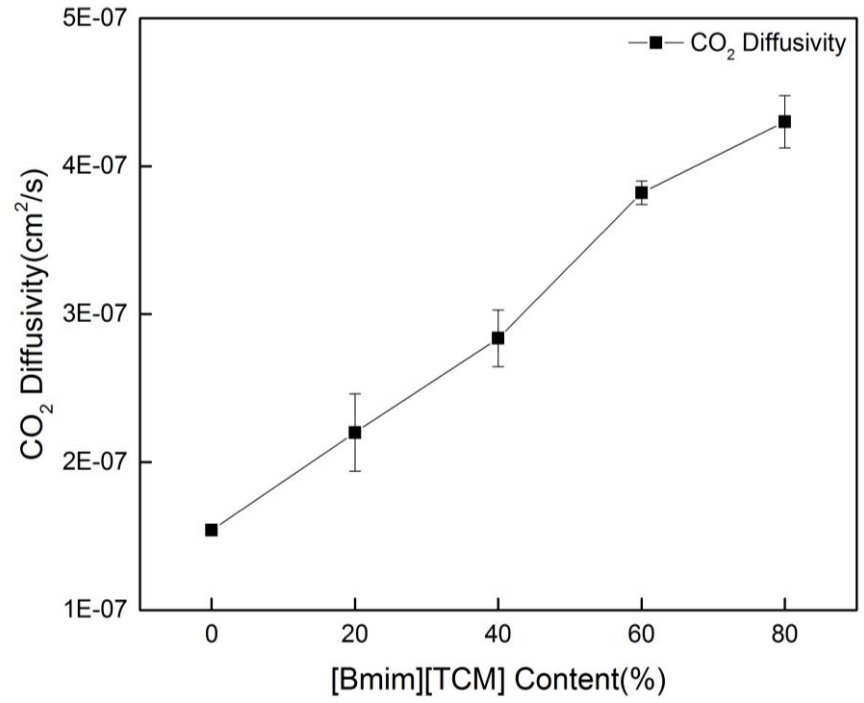

Figure 4.30 CO_2 Diffusivity of PEGDA/[Bmim][TCM] membrane with different [Bmim][TCM] content

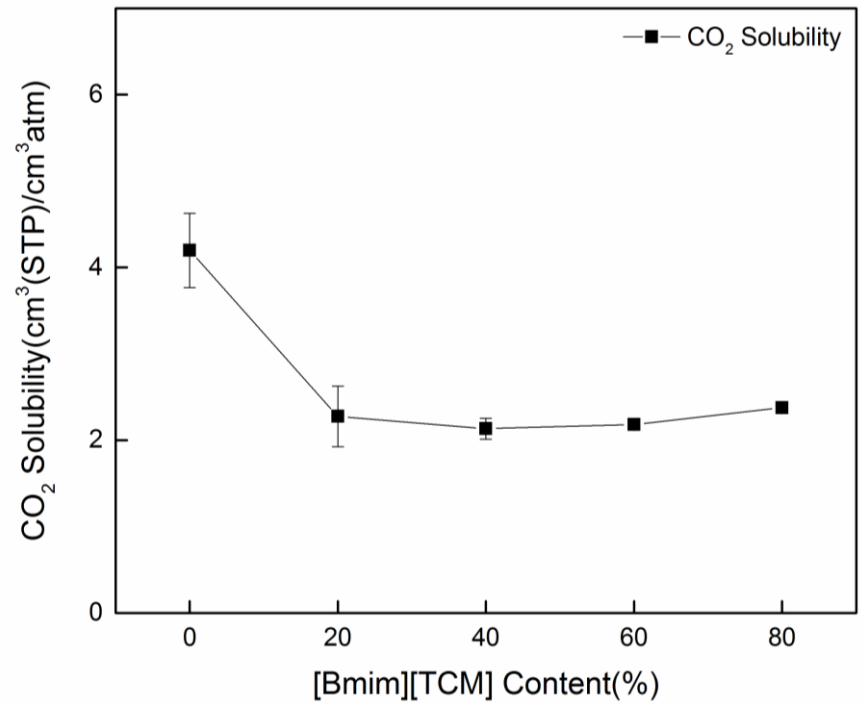

Figure 4.31 CO_2 Solubility of PEGDA/[Bmim][TCM] membrane with different [Bmim][TCM] content

CO_2 diffusivity and CO_2 solubility are calculated and showed in Figure 4.30 and 4.31 as a function of [Bmim][TCM] content. The diffusivity of CO_2 increases from 1.5 to 4.3×10^{-7} cm^2/s with the increasing of ionic liquid content from 0% to 80%. The 3-fold increment in CO_2 diffusivity is the result of plasticization of the polymer network by IL. Based on the result, it could be concluded the incorporated ionic liquid works as the plasticizer, improving the polymer chain mobility and may increasing the FFV of the cross-linked PEGDA membrane matrix. However, on the other side, CO_2 solubility displays a negative trend. By introducing the ionic liquid into the polymer matrix, the solubility declines from 4.1 to 2 $cm^3(STP)/cm^3atm$ which is approximately 50% of the neat cross-linked PEG membrane. When the ionic liquid content is more than 20%, the solubility is almost constant. This may be explained by the fact that the cross-linked

PEGDA membrane matrix has higher CO_2 affinity than [Bmim][TCM]. Since the permeability is the product of solubility and diffusivity, it is reasonable that CO_2 permeability drops when ionic liquid content is lower than 20%, while it increases at higher content. The idea CO_2/N_2 selectivity declines, but it still exhibits an acceptable level for CO_2 separation.

4.7 Summary of four PEGDA/IL membranes performance in Robeson graph

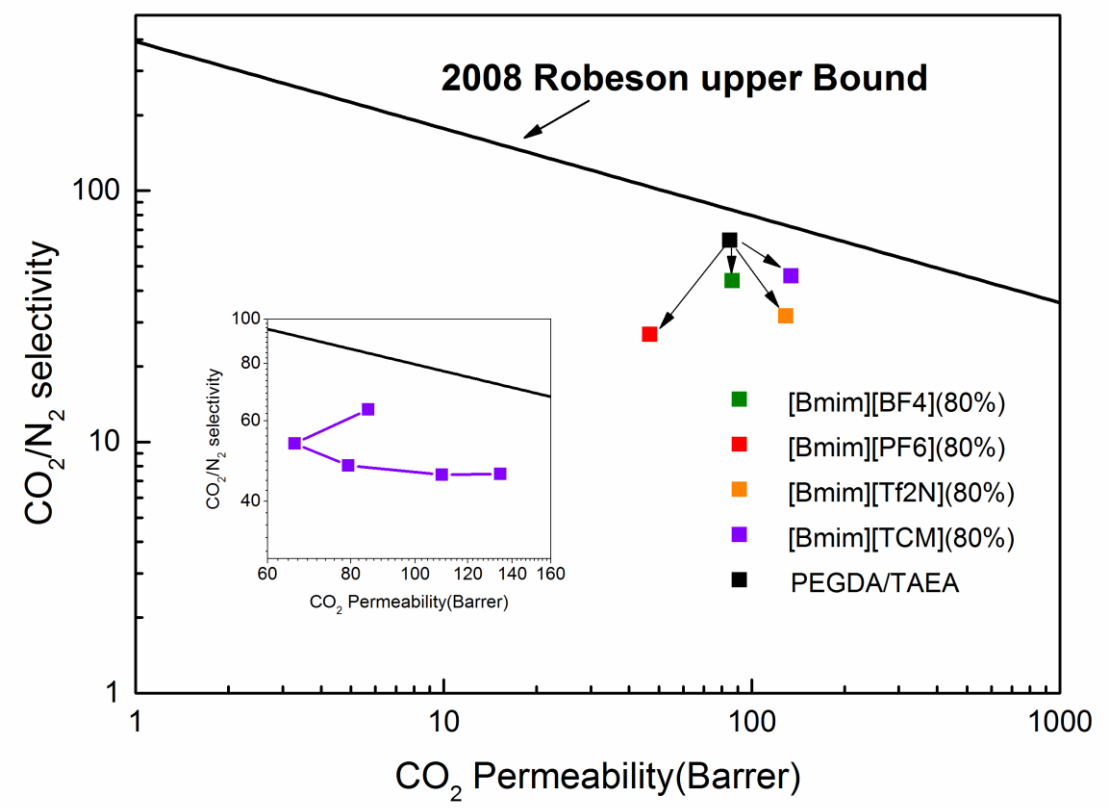

Figure 4.32 Separation performance results of PEGDA/IL membrane with different IL content at 1 bar and 24 °C compared with the Robeson upper bond curve

To get a clear overview of CO_2/N_2 separation performance of four different PEGDA/IL membranes, the CO_2 separation performance of the resultant membranes are compared with the Robeson upper bound. As can be seen in the figure, all the composite membranes are located near the upper bound expect these with [Bmim][PF_6]. Among four PEGDA/IL composite membranes, the performance of membranes blending with [Bmim][TCM] appears closest to the upper bond. Thereby, we can conclude PEGDA/[Bmim][TCM] membranes have the best performance in current work. The

moving path shown by arrows indicates different ionic liquid addition gives different effects on performance. For instance, [Bmim][PF_6] has a negative effect that the performance moves to the contrary direction as well as [Bmim][TCM] gives a positive effect that the performance moves to the more permeable direction. The effect of ionic liquid content on performance can also be analyzed conveniently. Four ionic liquids share the same trend. PEGDA/[Bmim][TCM] membranes are picked as an example and shown in the figure 4.32. When the membranes are with low ILs content, the loss of both permeability and selectivity leads the membranes performance away from the Robeson upper bound. Then due to the enhancement of permeability by further incorporation of the ionic liquid, the performance moves toward the right and gets closer to the upper bound.

5 Conclusion

The object of this work is to further improve the CO_2/N_2 separation performance of optimized cross-linked PEG-based membrane (XLPEGDA700/TAEA (6:1)) investigated in Specialization Project TKP 4580 2017. Four ionic liquids ([Bmim][BF_4], [Bmim][PF_6], [Bmim][Tf_2N] and [Bmim][TCM]) are chosen as additivities to enhance the gas transport property. XLPEGDA700/TAEA (6:1) membrane, which has the highest CO_2 permeability and CO_2/N_2 selectivity, is chosen as the membrane matrix.

FT-IR results confirm the mechanisms of aza-Michael addition between PEGDA and TAEA and homo-polymerization of acrylate group from PEGDA, as well as the presence of dual crosslinking networks. FT-IR results also reveal that four ionic liquids do not involve in two crosslinking reactions. In addition, for the composite membranes with [Bmim][BF_4], [Bmim][Tf_2N] and [Bmim][TCM], the increase in IL content is clearly observed in FT-IR results, while for the [Bmim][PF_6]-containing composite membranes with high content show irrelevance between IL content and peak intensity, suggesting the cross-linked PEG matrix may have a certain limitation for [Bmim][PF_6].

The thermal stability of composite membranes is investigated by TGA. Results show the thermal stability of the composite membranes is slightly reduced by the addition of ionic liquids. But still, all the membranes show excellent thermal stability for CO_2 separation in post-combustion, natural gas sweetening or other application, which are usually operated at a condition ranging from room temperature to 130 ^oC.

Phase transition behaviors of membranes are studied by DSC. For all the membranes, only one phase transition behavior between -45 to -55 ^{o}C can be observed. Slight reduction on T_g indicates the polymer chain flexibility is improved. XRD results suggest the cross-linked PEGDA/IL membranes are in the amorphous state at room temperature. The decline of peak intensity points out the crystallization of the membranes is decreasing by blending with ionic liquids. The water uptake results show the hydrophilicity of membranes is reduced by incorporation of ionic liquids. Among all composite membranes studied in this work, membranes with [Bmim][TCM] have the highest hydrophilicity.

Gas separation performance of these four composite membranes is also studied by single gas permeation tests. Permeability, diffusivity and solubility are obtained and calculated, as well as the CO_2/N_2 selectivity. Four ionic liquid composite membranes display the same trend: at low IL content, the CO_2 permeability decreases with incorporating ionic liquid. This is mainly because of the decrease in CO_2 solubility. With further addition of ionic liquid, CO_2 permeability increases as a result of the enhancement on diffusivity. Unlike CO_2 permeability, ideal CO_2/N_2 selectivity has a monotonous decline with increasing the ionic liquid content. Among four different ionic liquids, [Bmim][TCM] gives the best improvement on CO_2/N_2 separation performance among these IL-containing composite membranes. By adding 80% of [Bmim][TCM], CO_2 permeability increases from 85 to 138 Barrer with an acceptable decrease in selectivity from 63 to 45. Composite membrane blending with 80% of [Bmim][Tf_2N]

has a relative high CO_2 permeability of 129 Barrer and a moderate selectivity of 31.8. The addition of 80 % [Bmim][BF_4] in the polymer matrix does not improve the CO_2 permeability but slightly reduces the selectivity from 63.5 to 44. [Bmim][PF_6] has a negative effect both on CO_2 permeability and CO_2/N_2 selectivity. The composite membrane with 80% [Bmim][PF_6] has the lowest CO_2 permeability of 46.7 Barrer and the worst CO_2/N_2 selectivity of 26.8.

6 Future work

In this work, different ionic liquids acting as low molecular weight additive have different influence on membrane performance. By changing the chemical structure of ILs, the additive may lead to a significant improvement on gas transport properties. Besides ILs, free low-molecular-weight PEG is another promising additive due to its high affinity to CO_2. It is more CO_2-philic than the four ionic liquids used in this thesis. However, in this work, some preliminary results show that the added PEGDME (500 g/mol) is not stable inside this cross-linked PEG membranes. Due to the limited time, the optimization is not carried out. Therefore, in the further, some efforts may be worth carrying out by optimizing the molecular weight and end-group of free PEG.

Additionally, the functionalized ionic liquids might be another solution to further improve membrane performance. By introducing the suitable functional groups, blending TSILs, such as amino acid-based, amine-based and protic ionic liquid, into membranes may achieve much higher CO_2 separation performance than those with RTSLs. Due to the chemical absorption mechanisms, the composite membranes with TSILs might have better gas separation performance.

Reference

Ahn, S. H., Seo, J. A., Kim, J. H., Ko, Y., & Hong, S. U. (2009). Synthesis and gas permeation properties of amphiphilic graft copolymer membranes. *Journal of Membrane Science, 345*(1-2), 128-133.

Anthony, J. L., Anderson, J. L., Maginn, E. J., & Brennecke, J. F. (2005). Anion effects on gas solubility in ionic liquids. *The Journal of Physical Chemistry B, 109*(13), 6366-6374.

Baker, R. W. (2004). Membrane technology and applications. *John Wiley & Sons, Ltd*, 96-103.

Blanchard, L. A., Gu, Z., & Brennecke, J. F. (2001). High-pressure phase behavior of ionic liquid/CO2 systems. *The Journal of Physical Chemistry B, 105*(12), 2437-2444.

Car, A., Stropnik, C., Yave, W., & Peinemann, K.-V. (2008). Pebax®/polyethylene glycol blend thin film composite membranes for CO2 separation: Performance with mixed gases. *Separation and Purification Technology, 62*(1), 110-117.

Car, A., Stropnik, C., Yave, W., & Peinemann, K. V. (2008). Tailor‐made polymeric membranes based on segmented block copolymers for CO2 separation. *Advanced Functional Materials, 18*(18), 2815-2823.

Change, I. P. o. C. (2014). *Climate Change 2014–Impacts, Adaptation and Vulnerability: Regional Aspects*: Cambridge University Press.

Chen, H. Z., Li, P., & Chung, T.-S. (2012). PVDF/ionic liquid polymer blends with superior separation performance for removing CO2 from hydrogen and flue gas. *international journal of hydrogen energy, 37*(16), 11796-11804.

Dai, Z., Noble, R. D., Gin, D. L., Zhang, X., & Deng, L. (2016a). Combination of ionic liquids with membrane technology: A new approach for CO2 separation. *Journal of Membrane Science, 497*(Supplement C), 1-20. doi:https://doi.org/10.1016/j.memsci.2015.08.060

Dai, Z., Noble, R. D., Gin, D. L., Zhang, X., & Deng, L. (2016b). Combination of ionic liquids with membrane technology: A new approach for CO2 separation. *Journal of Membrane Science, 497*, 1-20.

Dlugokencky, E. a. T., P. (2017). Trends in atmospheric carbon dioxide. Retrieved

from https://www.esrl.noaa.gov/gmd/ccgg/trends/

Dong, L., Wang, Y., Chen, M., Shi, D., Li, X., Zhang, C., & Wang, H. (2016). Enhanced CO 2 separation performance of P (PEGMA-co-DEAEMA-co-MMA) copolymer membrane through the synergistic effect of EO groups and amino groups. *RSC Advances, 6*(65), 59946-59955.

Feng, S., Ren, J., Hua, K., Li, H., Ren, X., & Deng, M. (2013). Poly (amide-12-b-ethylene oxide)/polyethylene glycol blend membranes for carbon dioxide separation. *Separation and Purification Technology, 116*, 25-34.

Jiang, X., Li, S., & Shao, L. (2017). Pushing CO 2-philic membrane performance to the limit by designing semi-interpenetrating networks (SIPN) for sustainable CO 2 separations. *Energy & Environmental Science, 10*(6), 1339-1344.

Jindaratsamee, P., Ito, A., Komuro, S., & Shimoyama, Y. (2012). Separation of CO2 from the CO2/N2 mixed gas through ionic liquid membranes at the high feed concentration. *Journal of Membrane Science, 423*, 27-32.

Kanehashi, S., Kishida, M., Kidesaki, T., Shindo, R., Sato, S., Miyakoshi, T., & Nagai, K. (2013). CO2 separation properties of a glassy aromatic polyimide composite membranes containing high-content 1-butyl-3-methylimidazolium bis (trifluoromethylsulfonyl) imide ionic liquid. *Journal of Membrane Science, 430*, 211-222.

Kusuma, V. A., Macala, M. K., Liu, J., Marti, A. M., Hirsch, R. J., Hill, L. J., & Hopkinson, D. (2018). Ionic liquid compatibility in polyethylene oxide/siloxane ion gel membranes. *Journal of Membrane Science, 545*, 292-300.

Kusuma, V. A., Roth, E. A., Clafshenkel, W. P., Klara, S. S., Zhou, X., Venna, S. R., . . . Koepsel, R. R. (2015). Crosslinked poly (ethylene oxide) containing siloxanes fabricated through thiol‐ene photochemistry. *Journal of Polymer Science Part A: Polymer Chemistry, 53*(13), 1548-1557.

Kwisnek, L., Goetz, J., Meyers, K. P., Heinz, S. R., Wiggins, J. S., & Nazarenko, S. (2014). PEG Containing Thiol–Ene Network Membranes for CO2 Separation: Effect of Cross-Linking on Thermal, Mechanical, and Gas Transport Properties. *Macromolecules, 47*(10), 3243-3253.

Le Quéré, C., Andrew, R. M., Canadell, J. G., Sitch, S., Korsbakken, J. I., Peters, G. P., . . . Zaehle, S. (2016). Global Carbon Budget 2016. *Earth Syst. Sci. Data, 8*(2), 605-649. doi:10.5194/essd-8-605-2016

Lee, J. H., Hong, J., Kim, J. H., Kang, Y. S., & Kang, S. W. (2012). Facilitated CO 2 transport membranes utilizing positively polarized copper nanoparticles. *Chemical Communications, 48*(43), 5298-5300.

Lin, H., & Freeman, B. D. (2004). Gas solubility, diffusivity and permeability in poly (ethylene oxide). *Journal of Membrane Science, 239*(1), 105-117.

Lin, H., Kai, T., Freeman, B. D., Kalakkunnath, S., & Kalika, D. S. (2005). The effect of cross-linking on gas permeability in cross-linked poly (ethylene glycol diacrylate). *Macromolecules, 38*(20), 8381-8393.

Mannan, H. A., Mukhtar, H., Murugesan, T., Nasir, R., Mohshim, D. F., & Mushtaq, A. (2013). Recent applications of polymer blends in gas separation membranes. *Chemical Engineering & Technology, 36*(11), 1838-1846.

Metz, S., Mulder, M., & Wessling, M. (2004). Gas-permeation properties of poly (ethylene oxide) poly (butylene terephthalate) block copolymers. *Macromolecules, 37*(12), 4590-4597.

Mulder, J. (2012). *Basic principles of membrane technology*: Springer Science & Business Media.

Quan, S., Li, S., Wang, Z., Yan, X., Guo, Z., & Shao, L. (2015). A bio-inspired CO 2-philic network membrane for enhanced sustainable gas separation. *Journal of Materials Chemistry A, 3*(26), 13758-13766.

Rabiee, H., Ghadimi, A., & Mohammadi, T. (2015). Gas transport properties of reverse-selective poly (ether-b-amide6)/[Emim][BF4] gel membranes for CO2/light gases separation. *Journal of Membrane Science, 476*, 286-302.

Rao, A. B., & Rubin, E. S. (2002). A Technical, Economic, and Environmental Assessment of Amine-Based CO2 Capture Technology for Power Plant Greenhouse Gas Control. *Environmental Science & Technology, 36*(20), 4467-4475. doi:10.1021/es0158861

Robeson, L. M. (2008). The upper bound revisited. *Journal of Membrane Science, 320*(1-2), 390-400.

Rochelle, G. T. (2009). Amine Scrubbing for CO₂ Capture. *Science, 325*(5948), 1652.

Scovazzo, P., Kieft, J., Finan, D. A., Koval, C., DuBois, D., & Noble, R. (2004). Gas separations using non-hexafluorophosphate [PF6]− anion supported ionic liquid membranes. *Journal of Membrane Science, 238*(1-2), 57-63.

Shao, L., Quan, S., Cheng, X.-Q., Chang, X.-J., Sun, H.-G., & Wang, R.-G. (2013). Developing cross-linked poly (ethylene oxide) membrane by the novel reaction system for H2 purification. *international journal of hydrogen energy, 38*(12), 5122-5132.

Wang, S., Li, X., Wu, H., Tian, Z., Xin, Q., He, G., . . . Guiver, M. D. (2016). Advances in high permeability polymer-based membrane materials for CO2 separations. *Energy & Environmental Science, 9*(6), 1863-1890. doi:10.1039/C6EE00811A

White, R. P., & Lipson, J. E. (2016). Polymer free volume and its connection to the glass transition. *Macromolecules, 49*(11), 3987-4007.

Xue, B., Li, X., Gao, L., Gao, M., Wang, Y., & Jiang, L. (2012). CO 2-selective free-standing membrane by self-assembly of a UV-crosslinkable diblock copolymer. *Journal of Materials Chemistry, 22*(21), 10918-10923.

Yave, W., Car, A., & Peinemann, K.-V. (2010). Nanostructured membrane material designed for carbon dioxide separation. *Journal of Membrane Science, 350*(1-2), 124-129.

Zhao, Q., Leonhardt, E., MacConnell, C., Frear, C., & Chen, S. (2010). Purification technologies for biogas generated by anaerobic digestion. *Compressed Biomethane, CSANR, Ed*.

Zubeir, L. F., Romanos, G. E., Weggemans, W. M., Iliev, B., Schubert, T. J., & Kroon, M. C. (2015). Solubility and diffusivity of CO2 in the ionic liquid 1-butyl-3-methylimidazolium tricyanomethanide within a large pressure range (0.01 MPa to 10 MPa). *Journal of Chemical & Engineering Data, 60*(6), 1544-1562.